List of publications

This thesis is based on the following publications

Chapter 2

R. Kortlever, J. Shen, K.J.P. Schouten, F. Calle-Vallejo and M.T.M. Koper
Catalysts and reaction pathways for the electrochemical reduction of carbon dioxide
Journal of Physical Chemistry Letters, **2015**, *6*, 4073-4083.

Chapter 3

R. Kortlever, K.H. Tan, Y. Kwon and M.T.M. Koper
Electrochemical carbon dioxide and bicarbonate reduction on copper in weakly alkaline media
Journal of Solid State Electrochemistry, **2013**, *17*, 1843-1849.

Chapter 4

R. Kortlever, C. Balemans, Y. Kwon and M.T.M. Koper
Electrochemical CO_2 reduction to formic acid on a Pd-based formic acid oxidation catalyst
Catalysis Today, **2015**, *244*, 58-62.

Chapter 5

R. Kortlever, I. Peters, S. Koper and M.T.M. Koper
Electrochemical CO_2 reduction to formic acid at low overpotential and with high faradaic efficiencyon carbon-supported bimetallic Pd-Pt nanoparticles
ACS Catalysis, **2015**, *5*, 3916-3923.

Chapter 6

R. Kortlever, I. Peters, C. Balemans, R. Kas, Y. Kwon, G. Mul and M.T.M. Koper
A novel catalyst for the electrochemical reduction of CO_2 to C_1-C_5 hydrocarbons
Manuscript in preparation

Chapter 7

R. Kortlever, T.J.P. Hersbach, M. Koeman, M. Mulder, P. Bouwman and M.T.M Koper
Electrochemical CO_2 reduction to formic acid on $Pd_{70}Pt_{30}$ nanoparticles on different supports and in gas diffusion electrodes
Manuscript in preparation

Other publications

R. Kas, R. Kortlever, A. Milbrat. M.T.M. Koper, G. Mul and J. Baltrusaitis
Electrochemical CO_2 reduction on Cu_2O-derived copper nanoparticles: controlling the catalytic selectivity of hydrocarbons
Physical Chemistry Chemical Physics, **2014**, *16*, 12194-12201.

R. Kas, R. Kortlever, H. Yılmaz, M.T.M. Koper and G. Mul
Manipulating the Hydrocarbon Selectivity of Copper Nanoparticles in CO_2 Electroreduction by Process Conditions
ChemElectroChem, **2015**, *2*, 354-358.

J. Shen, R. Kortlever, R. Kas, Y.Y. Birdja, O. Diaz-Morales, Y. Kwon, I. Ledezma-Yanez, K.J.P. Schouten, G. Mul and M.T.M. Koper
Electrocatalytic reduction of carbon dioxide to carbon monoxide and methane at an immobilized cobalt protoporphyrin
Nature Communications, **2015**, *6*, 8177.

J. Monzó, Y. Malewski, R. Kortlever, F. J. Vidal-Iglesias, J. Solla-Gullón, M. T. M. Koper and P. Rodriguez
Enhanced electrocatalytic activity of Au@Cu core@shell nanoparticles towards CO_2 reduction
Journal of Materials Chemistry A, **2015**, DOI: 10.1039/C5TA06804E

R. Kas, K. Khazzal Hummadi, R. Kortlever, P. de Wit, A. Milbrat, M.W.J. Luiten-Olieman, N.E. Benes, M.T.M. Koper and G. Mul
CO_2 reduction with copper hollow fiber electrodes
Submitted for publication

O. Diaz-Morales, S. Raaijman, R. Kortlever, P.J. Kooyman, T. Wezendonk, J. Gascon, W.T. Fu and M.T. M. Koper
Iridium-based double perovskites for efficient water oxidation in acid media
Submitted for publication

B. Limburg, J. Wermink, S.S. van Nielen, R. Kortlever, M.T.M. Koper, E. Bouwman and S. Bonnet
Stabilization of a ruthenium photosensitizer for photocatalytic water oxidation by binding to a liposome bilayer
Manuscript in preparation

Curriculum vitae

Ruud Kortlever was born in Alblasserdam, The Netherlands on June 29th, 1987. After finishing his Gymnasium (high school) education at the Willem de Zwijger College in Papendrecht in 2005, he started his bachelor studies in Chemistry at Leiden University. During his bachelor he worked with dr. T.J. Mooibroek, prof. dr. E. Bouwman and prof. dr. E. Drent on transesterification reactions in an alternative route towards 4,4'-methylenediphenyldiisocyanate (MDI). He continued his education with a master study in Chemistry at Leiden University in the 'Research in Chemistry' track, with a specialization in 'Design and Synthesis'. During his master studies he worked as a summer research intern at Grinnell College in the summer of 2010, were he synthesized new ligands and new molybdenum di-imido, di-oxido and alkylidene complexes. In 2011 he completed his master studies with a thesis entitled 'Catalytic synthesis of primary amines via N-alkyl-formamide' under the supervision of dr. S. Raoufmoghaddam, prof. dr. E. Bouwman and prof. dr. E. Drent.

In November 2011 Ruud started his PhD project in the group of prof. dr. M.T.M. Koper, of which the results are presented in this thesis. During his PhD he collaborated with the groups of prof. dr. G. Mul at the University of Twente and dr. P. Rodriguez at the University of Birmingham. He presented his work during multiple national and international conferences and symposia for which he was awarded a presentation award and two poster awards.

Appendix I

Supporting information to Chapter 4

Appendix I.1 OLEMS measurements CO_2 reduction on Pd-Pt

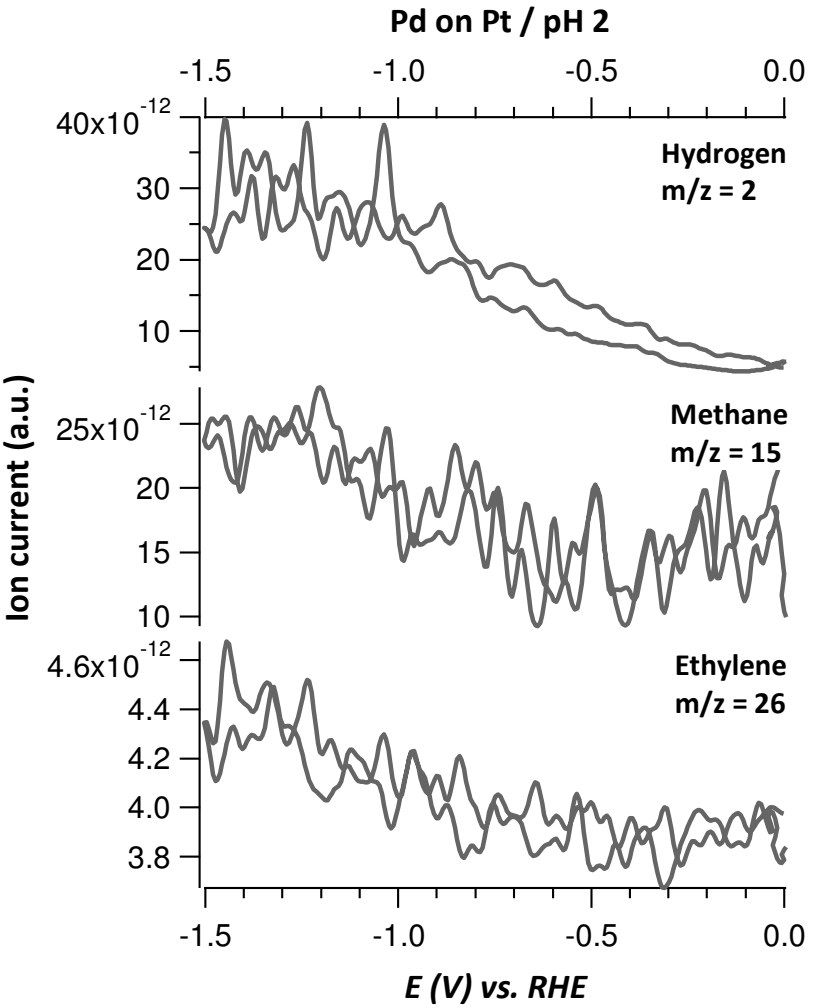

Figure AI.1 Formation of hydrogen (m/z = 2), methane (m/z = 15) and ethylene (m/z = 26) during CO_2 reduction on Pd-Pt followed with OLEMS in a pH 2 posphate buffer electrolyte (0.1 M H_3PO_4/ 0.1 M KH_2PO_4).

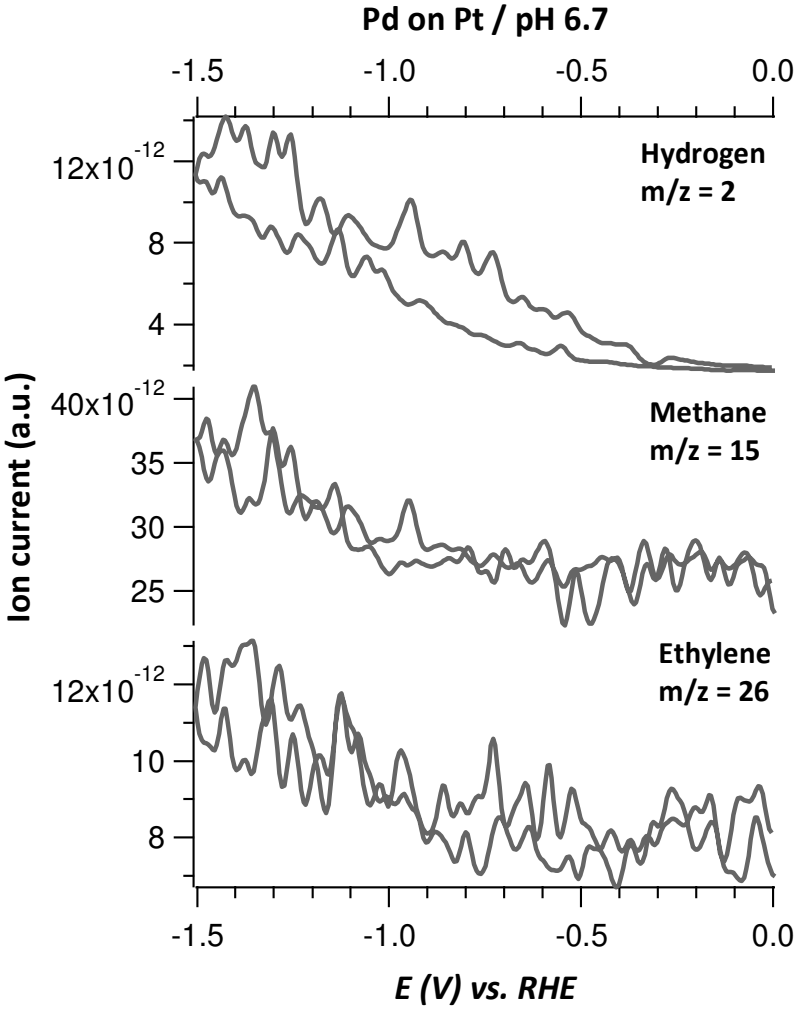

Figure AI.2 Formation of hydrogen (m/z = 2), methane (m/z = 15) and ethylene (m/z = 26) during CO_2 reduction on Pd-Pt followed with OLEMS in a pH 6.7 posphate buffer electrolyte (0.1 M K_2HPO_4/ 0.1 M KH_2PO_4).

Appendix I.2 Poisoning of the Pd-Pt electrode

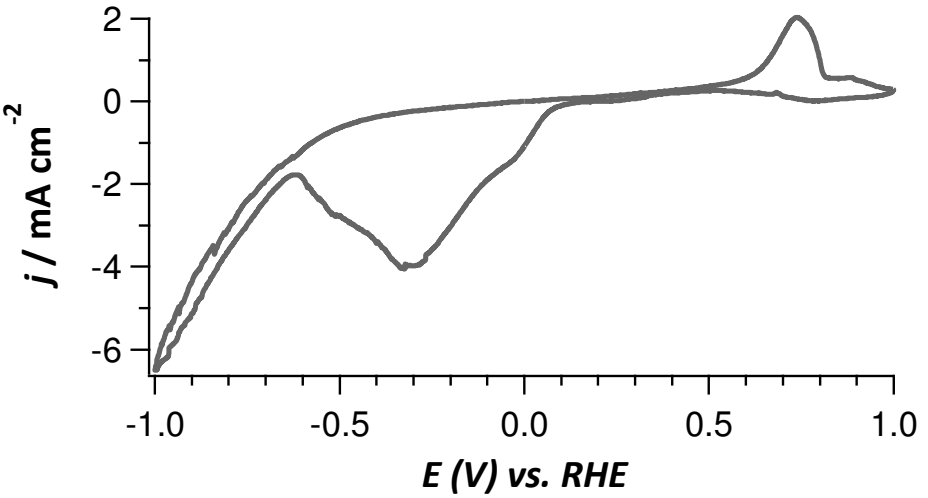

Figure AI.3 Cyclic voltammogram of a Pd-Pt electrode in a phosphate buffer at pH 6.7 (0.1 M KH_2PO_4 / 0.1 M K_2HPO_4) in the presence of CO_2 at a scan rate of 50 mV/s.

Appendix II

Supporting information to Chapter 5

Appendix II.1 Nanoparticle synthesis

Table AII.1 Volumes of K_2PdCl_4, K_2PtCl_4 and EDTA stock solutions used to synthesize a series of $Pd_xPt_{(100-x)}/C$ nanoparticles.

Composition	K_2PdCl_4 (0.05 M) / µl	K_2PtCl_4 (0.05 M) / µl	EDTA (0.1 M) / µl
Pd_5Pt_{95}/C	76	1430	753
$Pd_{10}Pt_{90}/C$	152	1354	753
$Pd_{20}Pt_{80}/C$	301	1205	753
$Pd_{30}Pt_{70}/C$	456	1050	753
$Pd_{40}Pt_{60}/C$	603	903	753
$Pd_{50}Pt_{50}/C$	753	753	753
$Pd_{60}Pt_{40}/C$	903	603	753
$Pd_{70}Pt_{30}/C$	1050	456	753
$Pd_{80}Pt_{20}/C$	1205	301	753
$Pd_{90}Pt_{10}/C$	1354	152	753
$Pd_{95}Pt_5/C$	1430	76	753
Pd/C	1506	0	753

Appendix II.2 IR compensation

Electrochemical impedance measurements were carried out prior to the long term electrolysis experiments to determine the resistance of the H-cell (see section S3). The impedance measurements were carried out using an Ivium A06075 potentiostat, at frequencies ranging from 10 kHz to 0.1 to measure the solution resistance. Since the resistance of the cell can vary for each experiment, it is important to correct for the resistance of the cell so that the applied potential during the electrolysis experiment corresponds to the intended electrode potential. A Nyquist plot was plotted as shown in Figure 1 and in the high-frequency part a linear fit was performed and the axis intersection was calculated. The value of this intersection represents the ohmic resistance of the cell. An average of 3 measurements was taken to calculate the value of R. Typically, very small resistances were measured, ranging from 3 to 10 Ω. This measured resistance was compensated for during the electrolysis experiments.

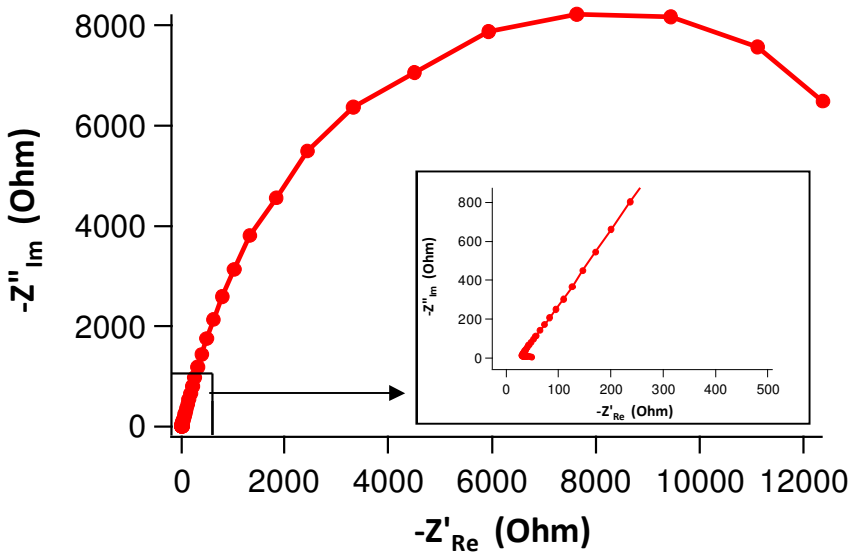

Figure AII.1 Typical Nyquist plot used to calculate the resictance of the cell prior to electrolysis experiments.

Appendix II.3 Faradaic efficiency

Faradaic efficiency measurements were performed in a custom-made H-cell over the course of 2 hours. Every 10 minutes a sample of 100 µl was taken from the cathodic compartment. These samples were analyzed with HPLC to determine the concentration of formic acid. During the 10 minutes of electrolysis current-time plots were made, that were used afterwards to calculate the total charge (C) that was consumed. Since every molecule of formic acid is produced from CO_2 plus $2e^-$, the partial charge of formic acid could be calculated from the amount of formic acid that was produced multiplied with 2 times the elementary charge of an electron (e). The faradaic efficiency was then determined by dividing the partial charge for formic acid by the total amount of charge that was consumed, as shown in Equation 1. The FE was calculated for the different nanoparticle compositions.

$$FE = \frac{[\text{Formic Acid}] \cdot 2e}{\sum \text{Charge}} \cdot 100\% \quad (1)$$

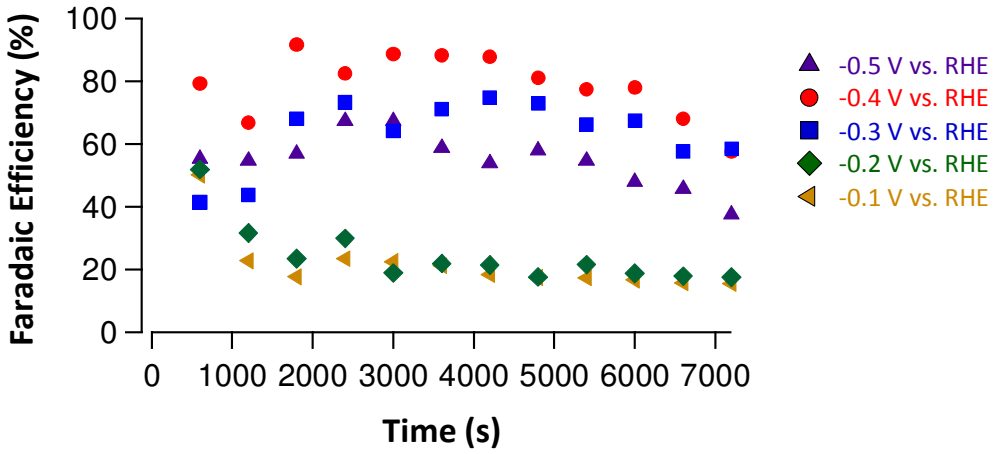

Figure AII.2 Faradaic efficiencies for formic acid production from CO_2 on $Pd_xPt_{(100-x)}$/C nanoparticles in a 0.1 M K_2HPO_4 / 0.1 KH_2PO_4 electrolyte (pH 6.7) that was saturated with CO_2 at potentials ranging from 0 V vs. RHE to -0.5 V vs. RHE (the applied potential was corrected for the cell resistance). The experiments were conducted for 2 hours, while samples of the electrolyte were taken every 10 minutes.

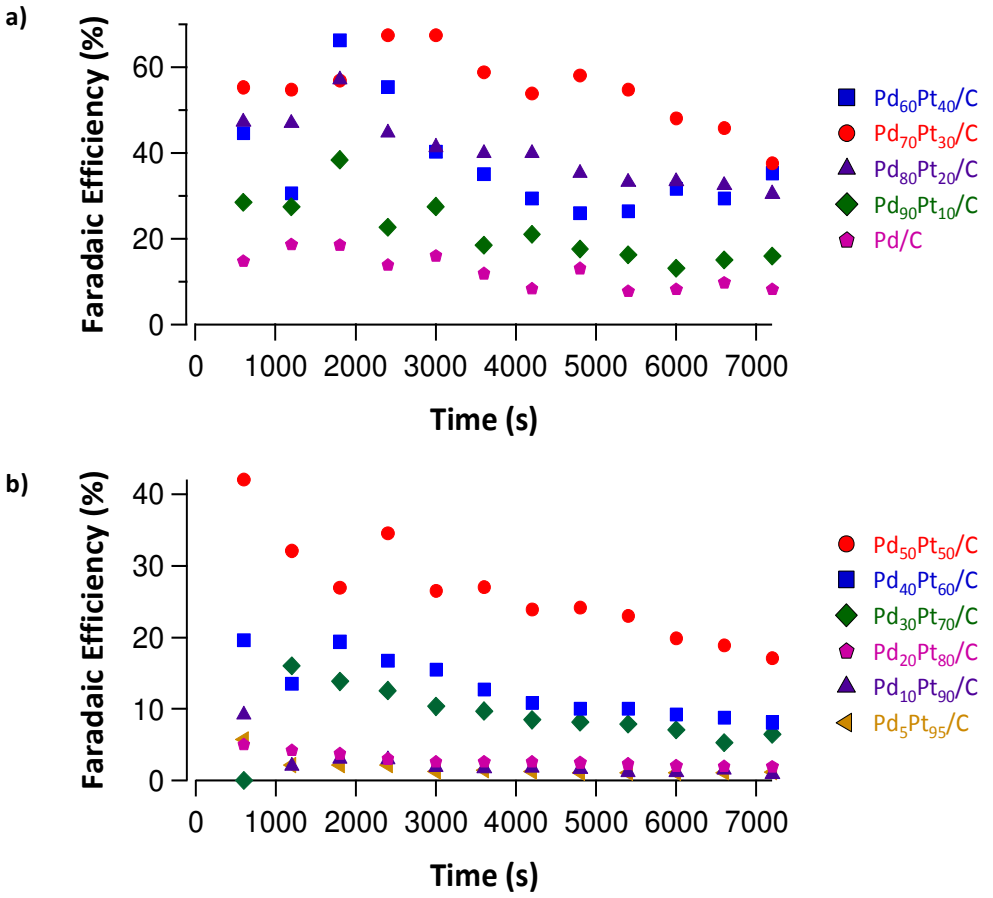

Figure AII.3 Faradaic efficiencies for formic acid production from CO_2 on $Pd_xPt_{(100-x)}/C$ nanoparticles in a 0.1 M K_2HPO_4 / 0.1 KH_2PO_4 electrolyte (pH 6.7) that was saturated with CO_2. The electrolysis experiments were conducted at -0.5 V vs. RHE (the applied potential was corrected for the cell resistance) in. The experiments were conducted for 2 hours, while samples of the electrolyte were taken every 10 minutes.

Table AII.2 Tabulated faradaic efficiency values for CO_2 reduction to formic acid on Pd_5Pt_{95}/C to $Pd_{50}Pt_{50}$/C nanoparticles over the course of 2 hours.

Time (s)	**Pd_5Pt_{95}/C** FE (%)	**$Pd_{10}Pt_{90}$/C** FE (%)	**$Pd_{20}Pt_{80}$/C** FE (%)	**$Pd_{30}Pt_{70}$/C** FE (%)	**$Pd_{40}Pt_{60}$/C** FE (%)	**$Pd_{50}Pt_{50}$/C** FE (%)
600	5.8	9.3	5.0	0.0	19.6	42.0
1200	2.2	2.1	4.3	16.1	13.6	32.1
1800	2.2	3.1	3.8	13.9	19.4	26.9
2400	2.1	3.0	3.0	12.6	16.7	34.5
3000	1.3	1.9	2.6	10.4	15.5	26.5
3600	1.5	1.7	2.6	9.7	12.8	27.0
4200	1.3	1.8	2.6	8.5	10.9	23.9
4800	1.1	1.7	2.5	8.2	10.1	24.2
5400	1.1	1.2	2.3	7.9	10.0	23.0
6000	1.1	1.2	2.0	7.1	9.2	19.9
6600	1.1	1.5	2.0	5.3	8.8	18.9
7200	1.2	0.9	1.9	6.5	8.1	17.1

Table AII.3 Tabulated faradaic efficiency values for CO_2 reduction to formic acid on $Pd_{60}Pt_{40}$/C to Pd/C nanoparticles over the course of 2 hours.

Time (s)	**$Pd_{60}Pt_{40}$/C** FE (%)	**$Pd_{70}Pt_{30}$/C** FE (%)	**$Pd_{80}Pt_{20}$/C** FE (%)	**$Pd_{90}Pt_{10}$/C** FE (%)	**$Pd_{95}Pt_5$/C** FE (%)	**Pd/C** FE (%)
600	44.6	55.3	47.2	28.5	40.5	14.7
1200	30.5	54.7	46.9	27.4	58.9	18.6
1800	66.3	56.9	57.1	38.4	52.5	18.5
2400	55.4	67.4	44.7	22.6	53.3	13.8
3000	40.3	67.4	41.4	27.5	42.4	16.0
3600	35.1	58.8	39.9	18.5	35.1	11.8
4200	29.4	53.9	40.0	21.0	37.0	8.2
4800	25.9	58.1	35.3	17.6	45.7	13.0
5400	26.4	54.7	33.1	16.3	33.7	7.7
6000	31.7	48.1	33.3	13.2	31.1	8.1
6600	29.4	45.8	32.4	15.0	32.5	9.7
7200	35.3	37.6	30.4	16.0	29.4	8.2

Table AII.4 Tabulated faradaic efficiency values for CO_2 reduction to formic acid on $Pd_{70}Pt_{30}$/C nanoparticles at different potentials over the course of 2 hours.

Time (s)	**-0.1 V vs. RHE** FE (%)	**-0.2 V vs. RHE** FE (%)	**-0.3 V vs. RHE** FE (%)	**-0.4 V vs. RHE** FE (%)	**-0.5 V vs. RHE** FE (%)
600	51.9	50.1	41.5	79.4	55.3
1200	31.6	22.7	43.8	66.8	54.7
1800	23.4	17.7	68.1	91.8	56.9
2400	29.9	23.4	73.3	82.5	67.4
3000	18.8	22.5	64.2	88.8	67.4
3600	21.9	21.2	71.3	88.4	58.8
4200	21.4	18.4	74.8	87.9	53.9
4800	17.6	17.4	73.1	81.1	58.1
5400	21.6	17.3	66.3	77.5	54.7
6000	18.7	16.6	67.5	78.0	48.1
6600	17.8	15.8	57.6	68.2	45.8
7200	17.5	15.5	58.6	57.6	37.6

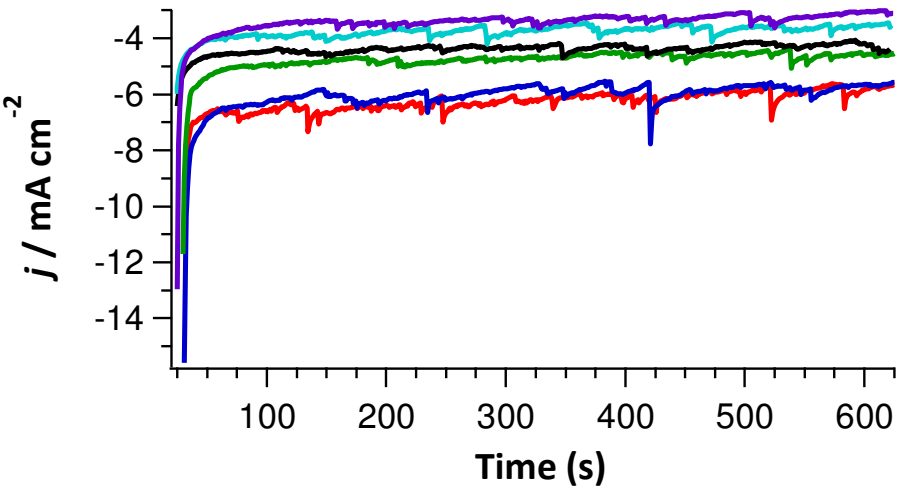

Figure AII.4 Current vs. time plot for electrolysis on $Pd_{70}Pt_{30}$/C at -0.4 V vs. RHE in a pH 6.7 phosphate buffer (0.1 M K_2HPO_4 / 0.1 KH_2PO_4) at different electrolysis times; between 0-10 minutes (red), between 10-20 minutes (blue), between 40-50 minutes (green), between 50-60 minutes (black), between 100-110 minutes (cyan) and between 110-120 minutes (purple).

Appendix II.4 TEM data of $Pd_xPt_{(100-x)}$/C nanoparticles

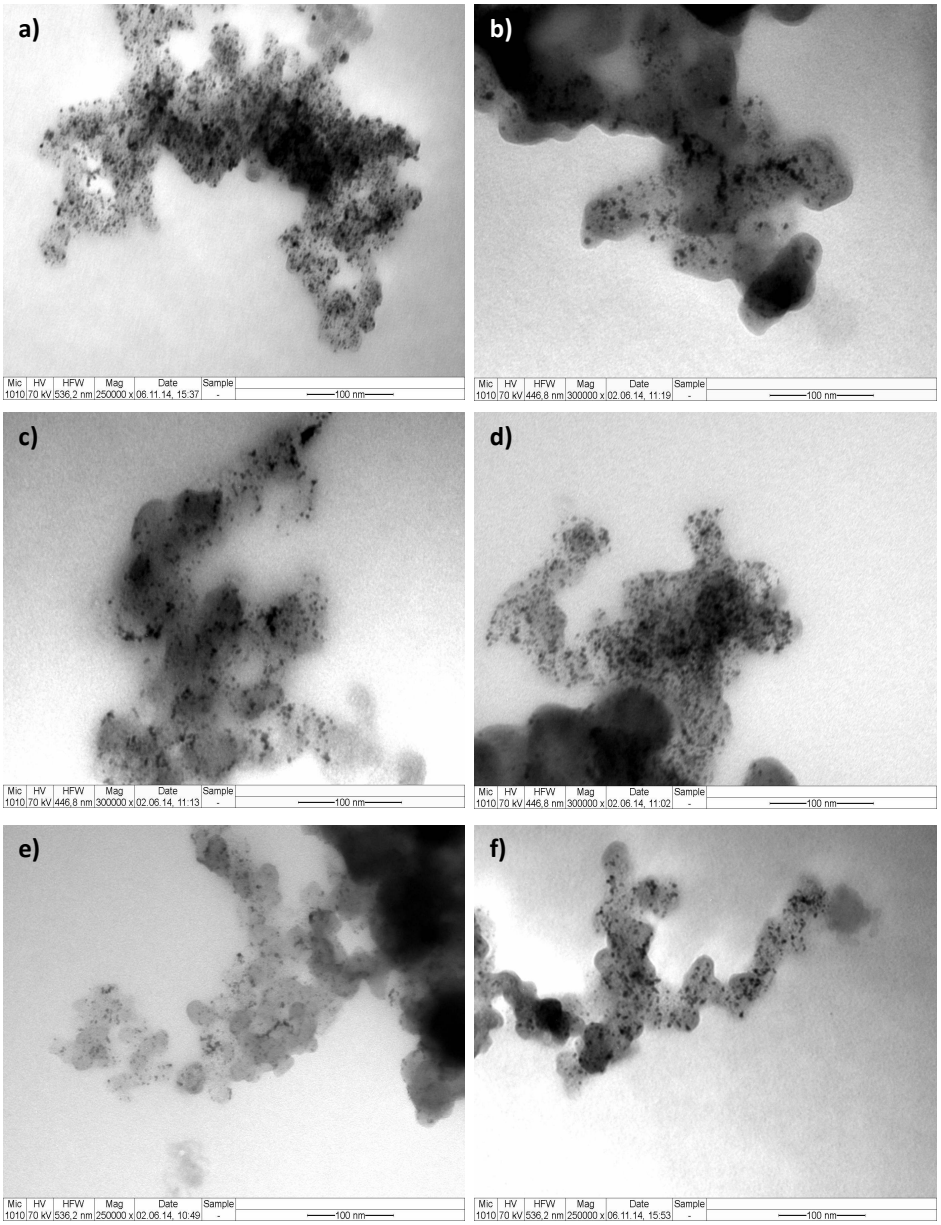

Figure AII.5 Transmission electron microscopy (TEM) images of: **a)** Pd_5Pt_{95}/C, **b)** $Pd_{10}Pt_{90}$/C, **c)** $Pd_{20}Pt_{80}$/C, **d)** $Pd_{30}Pt_{70}$/C, **e)** $Pd_{40}Pt_{60}$/C and **f)** $Pd_{50}Pt_{50}$/C.

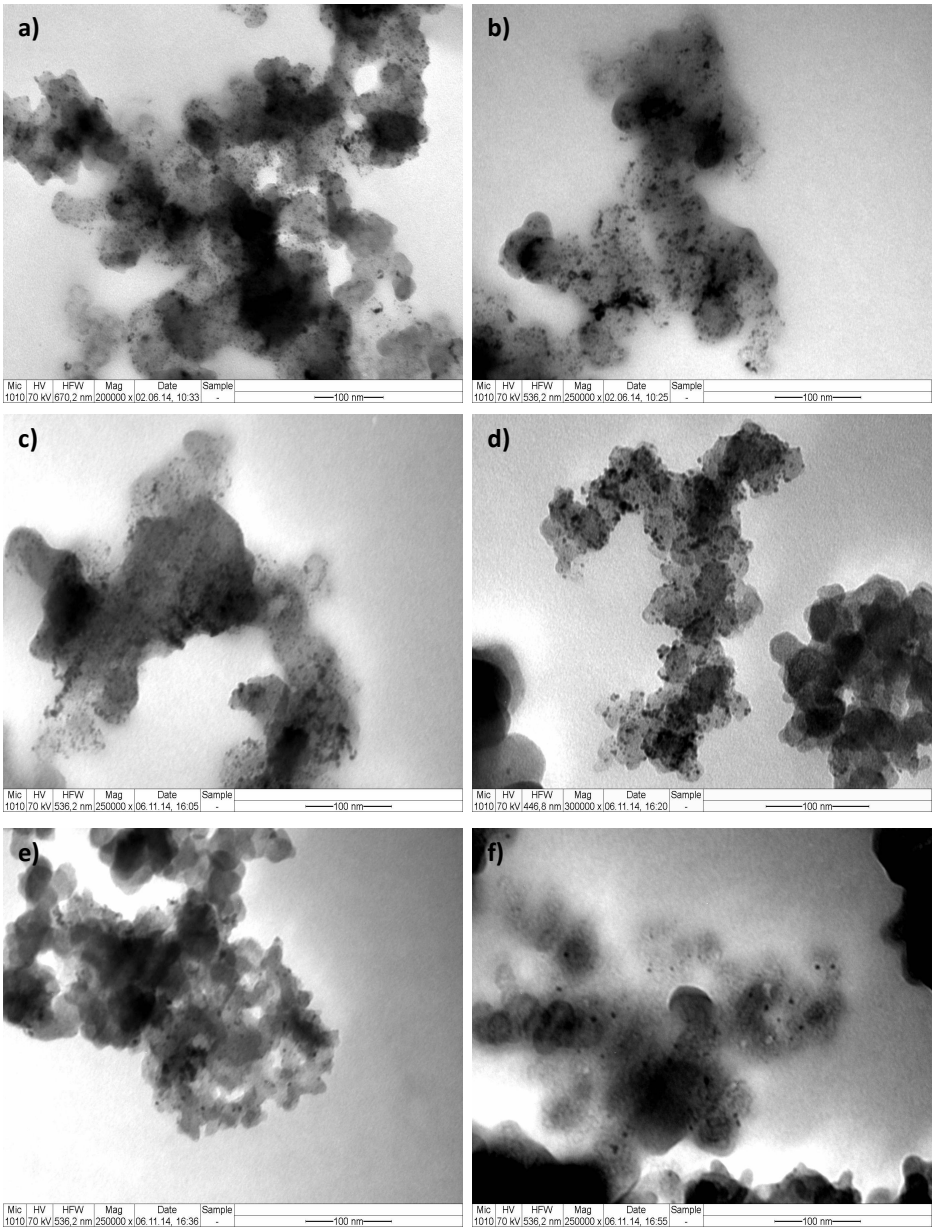

Figure AII.6 Transmission electron microscopy (TEM) images of: **a)** $Pd_{60}Pt_{40}$/C, **b)** $Pd_{70}Pt_{30}$/C, **c)** $Pd_{80}Pt_{20}$/C, **d)** $Pd_{90}Pt_{10}$/C, **e)** $Pd_{95}Pt_{5}$/C and **f)** Pd/C.

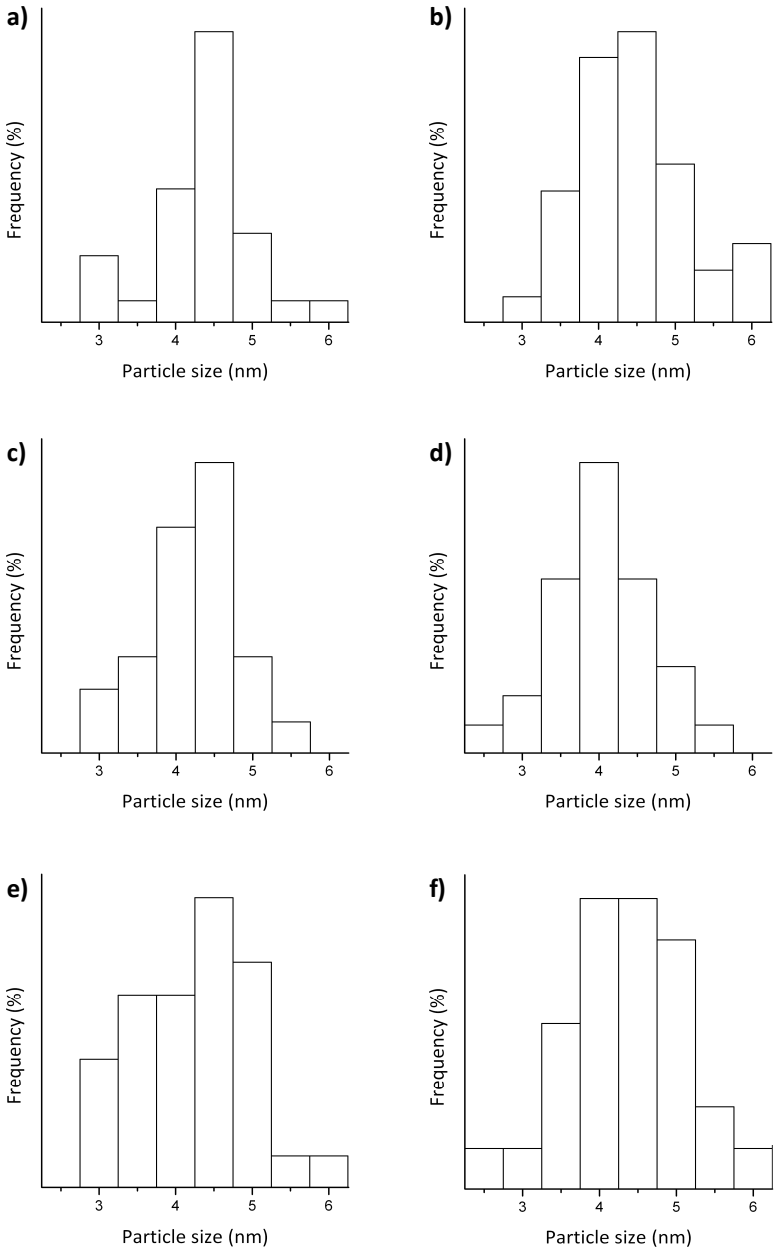

Figure AII.7 Particle size distribution histograms of: **a)** Pd_5Pt_{95}/C, **b)** $Pd_{10}Pt_{90}$/C, **c)** $Pd_{20}Pt_{80}$/C, **d)** $Pd_{30}Pt_{70}$/C, **e)** $Pd_{40}Pt_{60}$/C and **f)** $Pd_{50}Pt_{50}$/C.

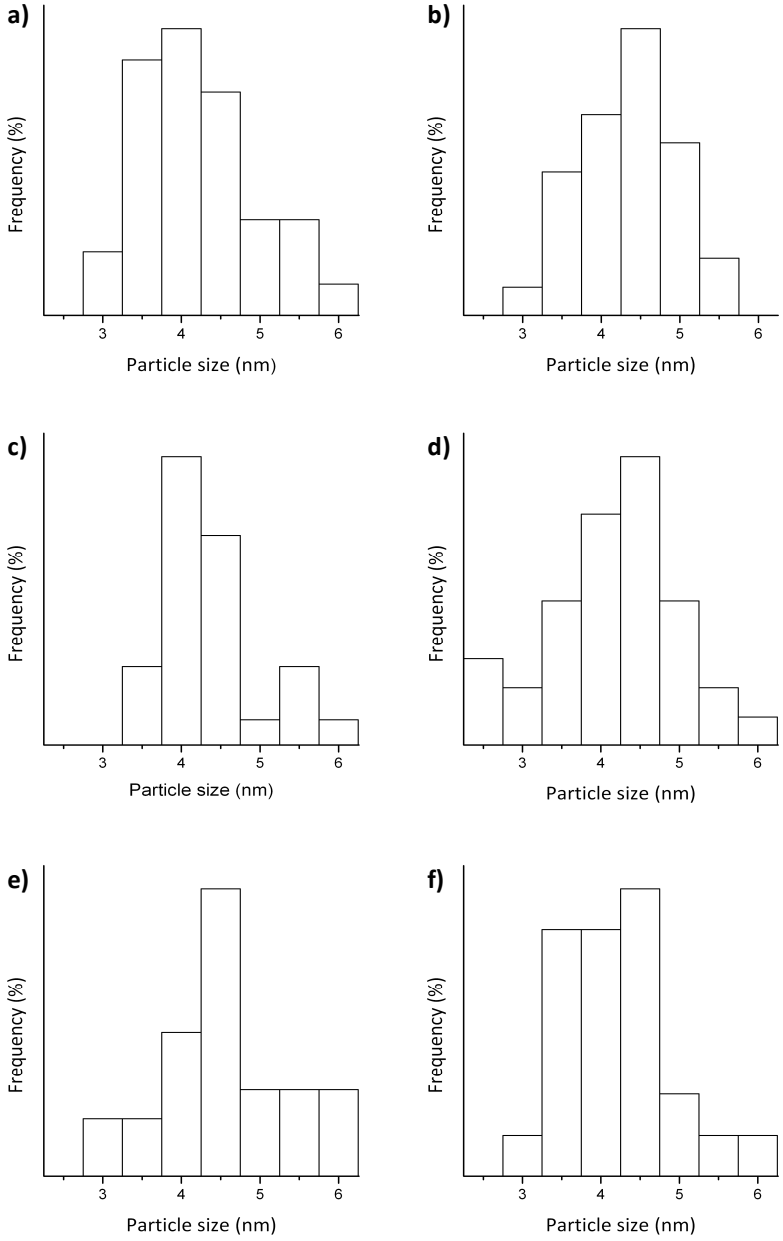

Figure AII.8 Particle size distribution histograms of: **a)** $Pd_{60}Pt_{40}$/C, **b)** $Pd_{70}Pt_{30}$/C, **c)** $Pd_{80}Pt_{20}$/C, **d)** $Pd_{90}Pt_{10}$/C, **e)** $Pd_{95}Pt_{5}$/C and **f)** Pd/C.

Appendix II.5 CO_2 reduction and blank voltammetry on $Pd_xPt_{(100-x)}$

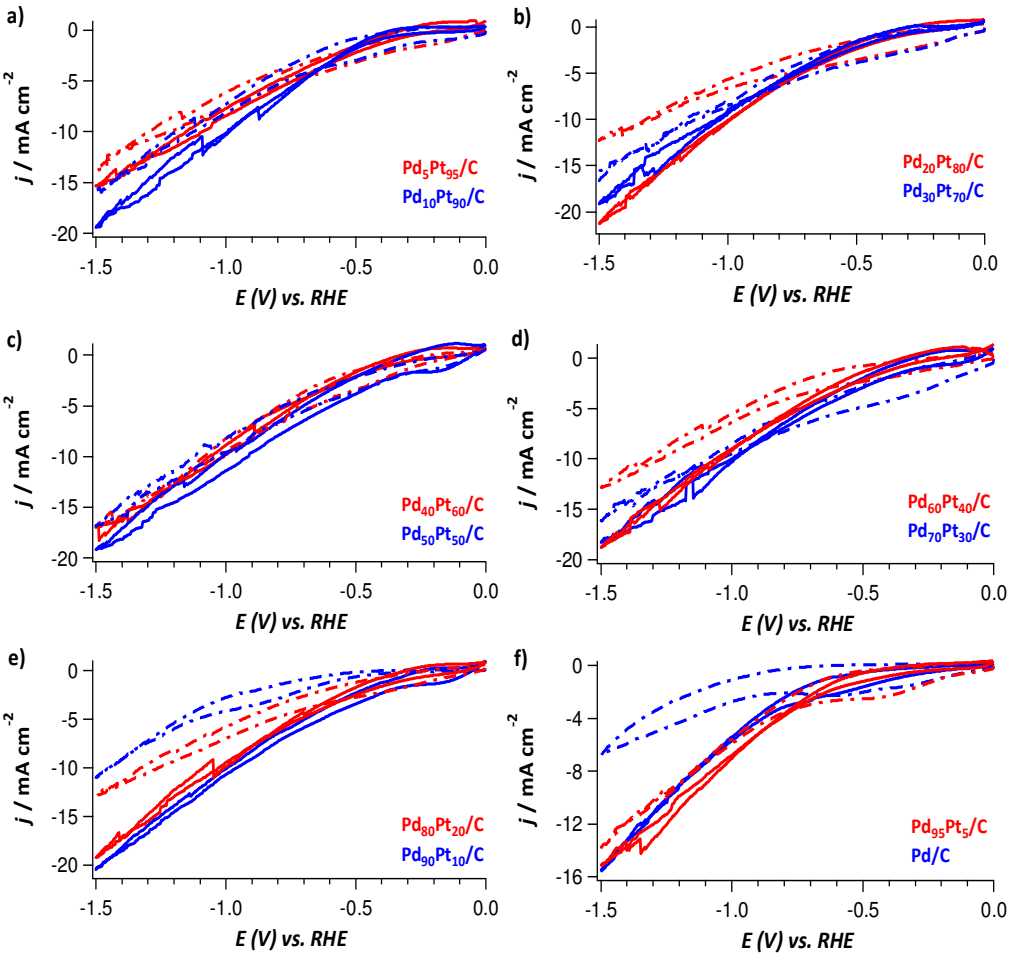

Figure AII.9 Cyclic voltammograms of $Pd_xPt_{(100-x)}$/C nanoparticles recorded in a 0.1 M KH_2PO_4 / 0.1 M K_2HPO_4 electrolyte (pH 6.7) at a scan rate of 50 mV/s purged with either argon (solid lines) or CO_2 (dashed lines); Cyclic voltammograms of **a)** Pd_5Pt_{95}/C (red) and $Pd_{10}Pt_{90}$/C (blue); **b)** $Pd_{20}Pt_{80}$/C (red) and $Pd_{30}Pt_{70}$/C (blue); **c)** $Pd_{40}Pt_{60}$/C (red) and $Pd_{50}Pt_{50}$/C (blue); **d)** $Pd_{60}Pt_{40}$/C (red) and $Pd_{70}Pt_{30}$/C (blue); **e)** $Pd_{80}Pt_{20}$/C (red) and $Pd_{90}Pt_{10}$/C (blue); **f)** $Pd_{95}Pt_5$/C (red) and Pd/C (blue).

Appendix III

Supporting information to Chapter 6

Appendix IV.1 SEM images PdAu electrodes

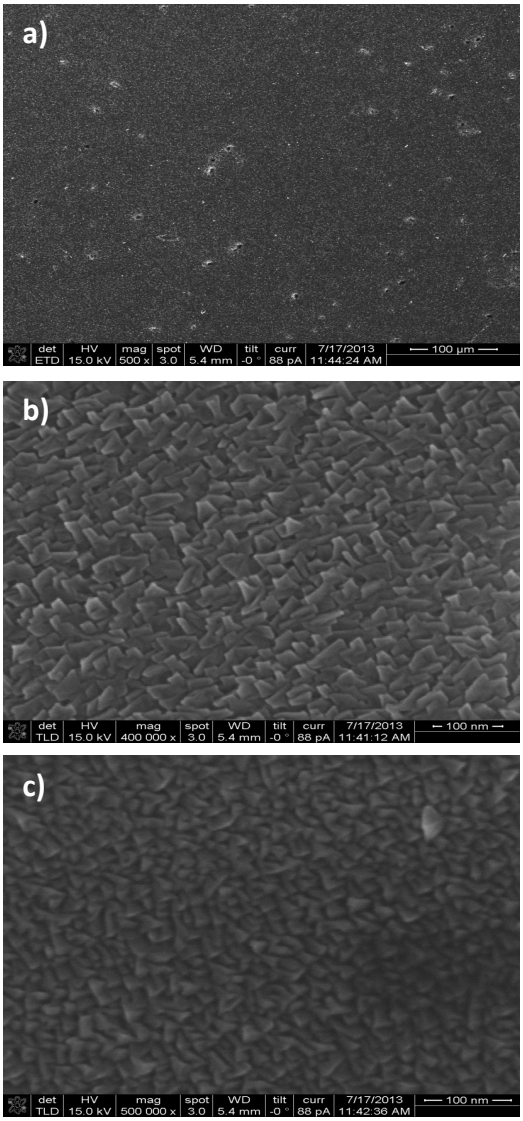

Figure AIII.1 Scanning electron microscopy (SEM) images of palladium overlayers electrodeposited on a gold electode at different magnifications; **a)** overview of the deposition layer , **b)** scale-like structure, **c)** triangular structure.

Appendix III.2 Additional OLEMS data

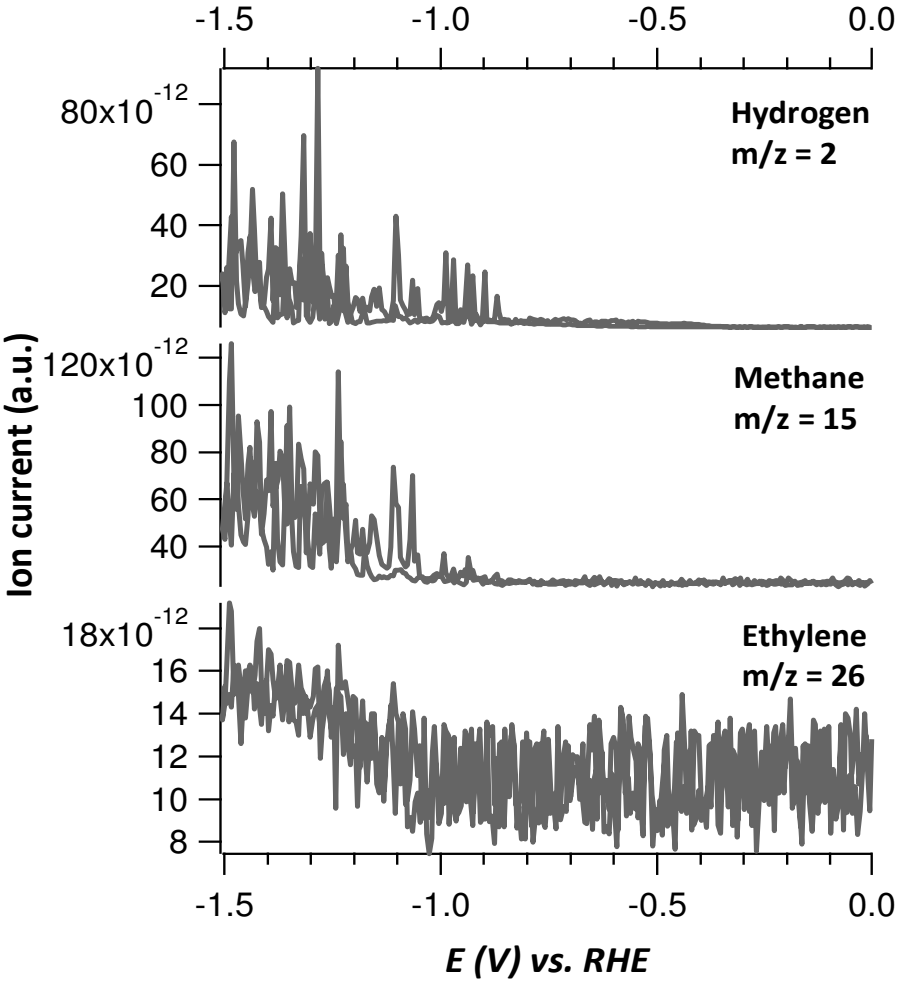

Figure AIII.2 Formation of hydrogen (m/z = 2), methane (m/z = 15) and ethylene (m/z = 26) from CO_2 reduction on a polycrystalline palladium electrode followed with OLEMS in a pH 6.7 phosphate buffer electrolyte (0.1 M KH_2PO_4/ 0.1 M K_2HPO_4).

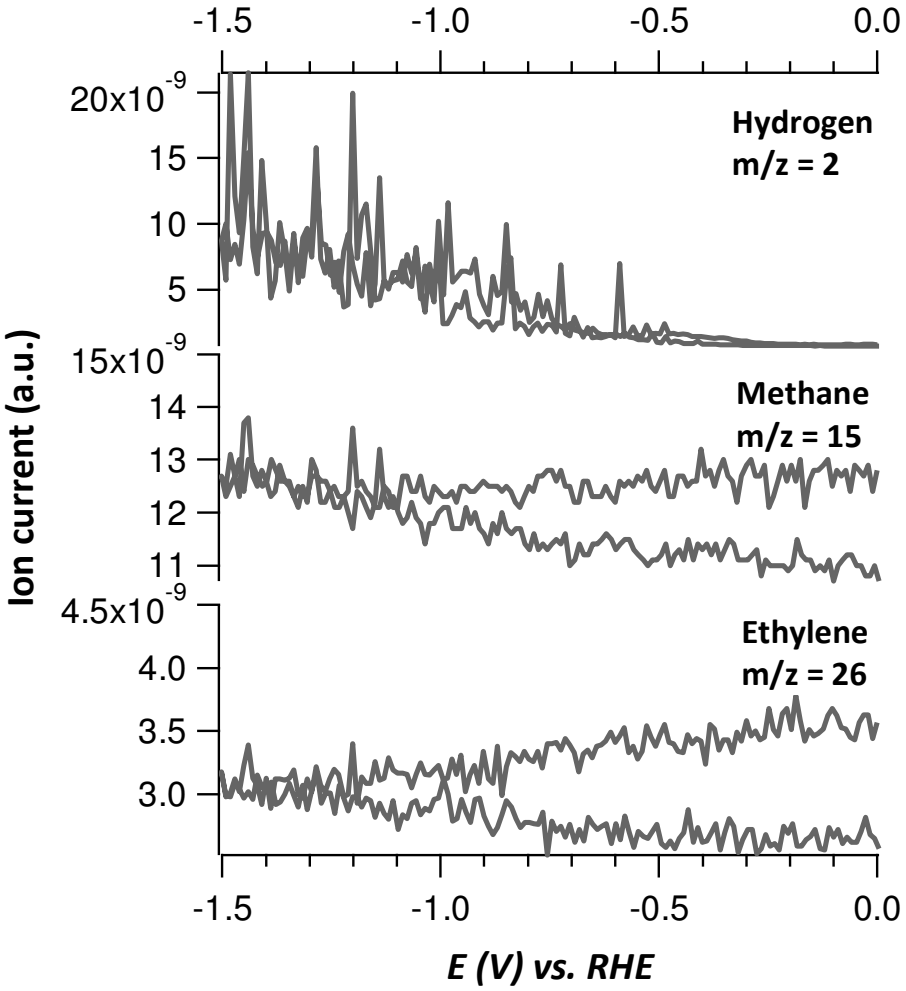

Figure AIII.3 Formation of hydrogen (m/z = 2), methane (m/z = 15) and ethylene (m/z = 26) from CO_2 reduction on a polycrystalline gold electrode followed with OLEMS in a pH 6.7 phosphate buffer electrolyte (0.1 M KH_2PO_4/ 0.1 M K_2HPO_4).

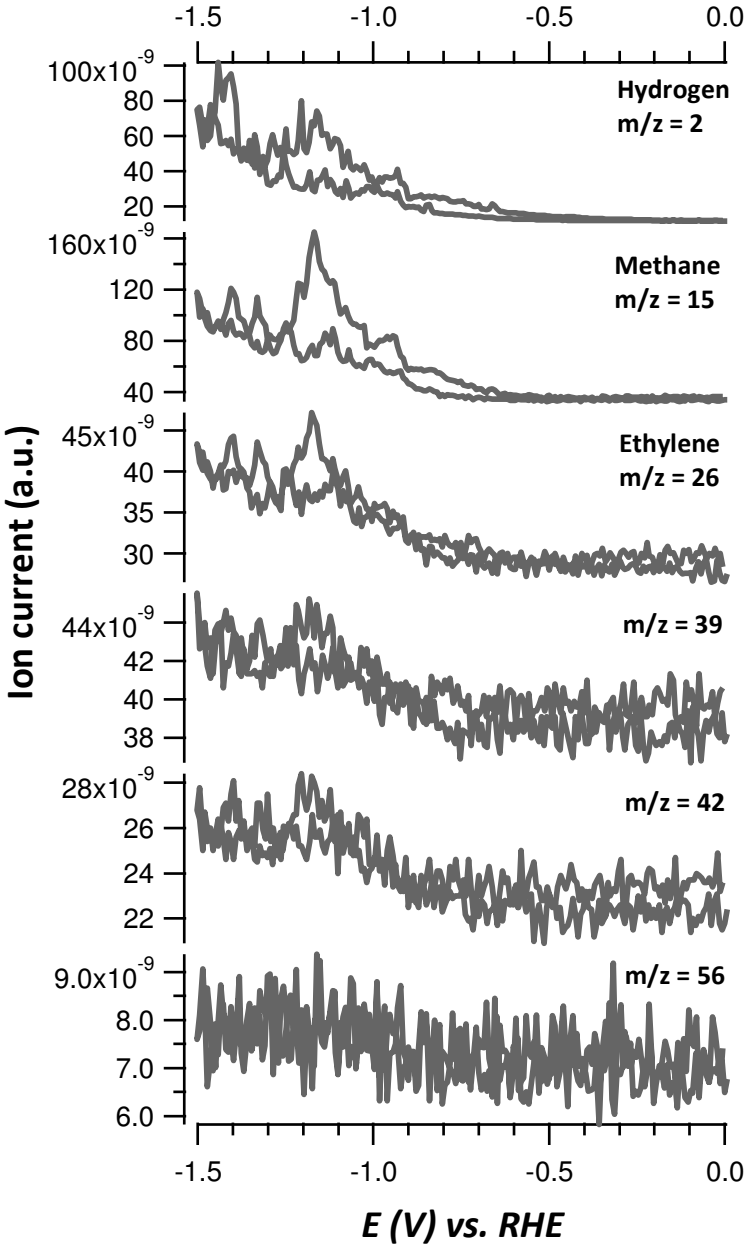

Figure AIII.4 Formation of hydrogen (m/z = 2), methane (m/z = 15) ethylene (m/z = 26), C_3 hydrocarbons (m/z = 39 and 42) and C_4 hydrocarbons (m/z = 56) from CO_2 reduction on a polycrystalline gold electrode covered with 1 palladium ML followed with OLEMS in a pH 6.7 phosphate buffer electrolyte (0.1 M KH_2PO_4/ 0.1 M K_2HPO_4).

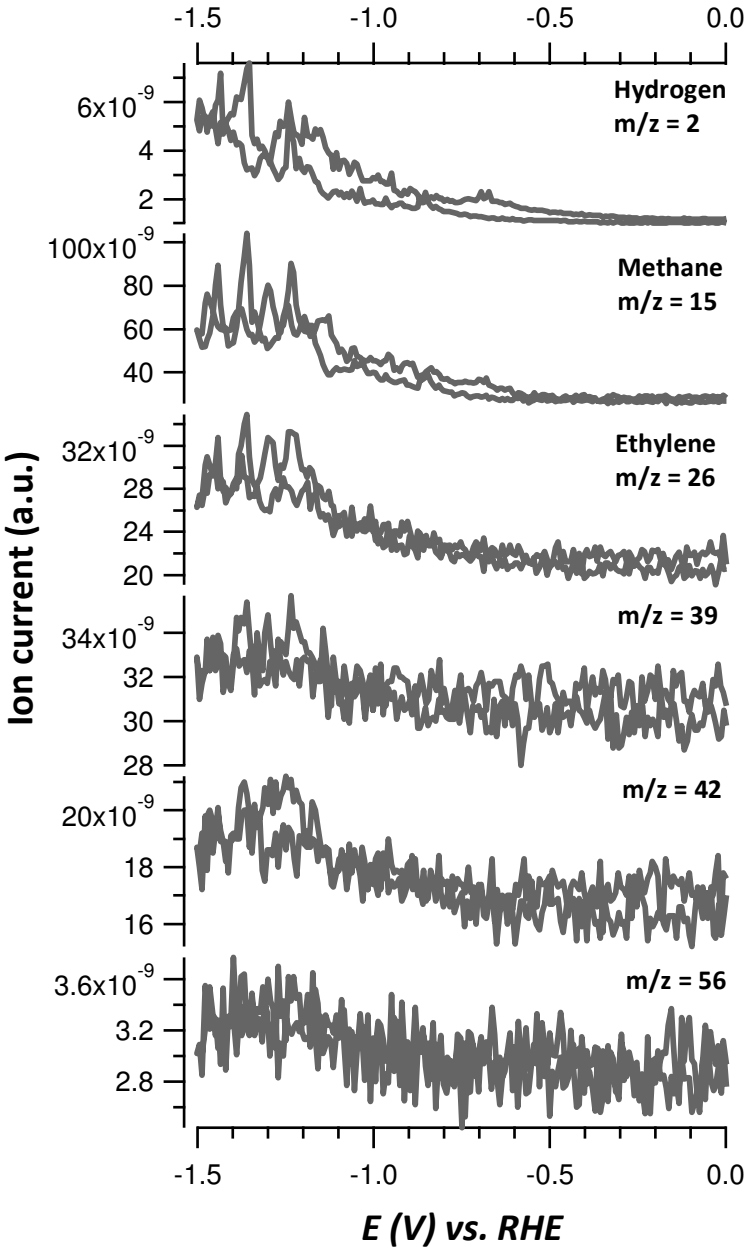

Figure AIII.5 Formation of hydrogen (m/z = 2), methane (m/z = 15) ethylene (m/z = 26), C_3 hydrocarbons (m/z = 39 and 42) and C_4 hydrocarbons (m/z = 56) from CO_2 reduction on a polycrystalline gold electrode covered with 2 palladium ML followed with OLEMS in a pH 6.7 phosphate buffer electrolyte (0.1 M KH_2PO_4/ 0.1 M K_2HPO_4).

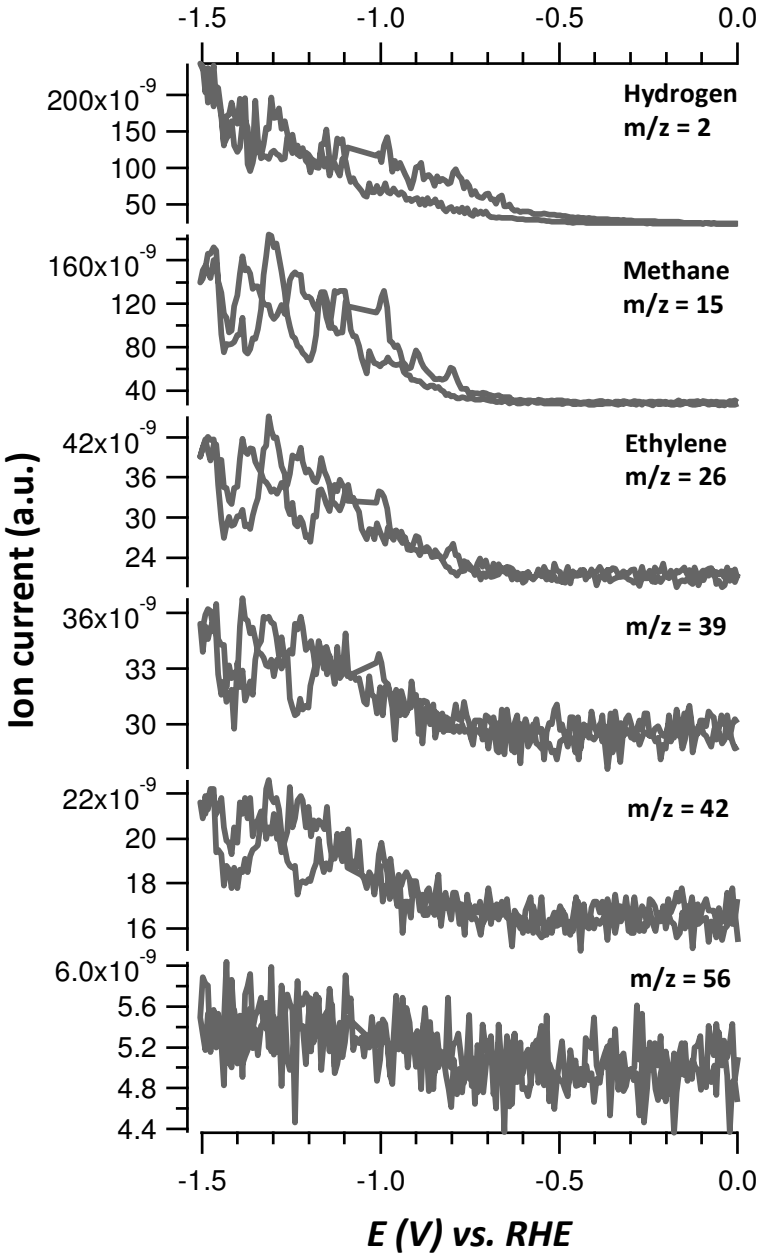

Figure AIII.6 Formation of hydrogen (m/z = 2), methane (m/z = 15) ethylene (m/z = 26), C_3 hydrocarbons (m/z = 39 and 42) and C_4 hydrocarbons (m/z = 56) from CO_2 reduction on a polycrystalline gold electrode covered with 3 palladium ML followed with OLEMS in a pH 6.7 phosphate buffer electrolyte (0.1 M KH_2PO_4/ 0.1 M K_2HPO_4).

Appendix III.3 Online HPLC

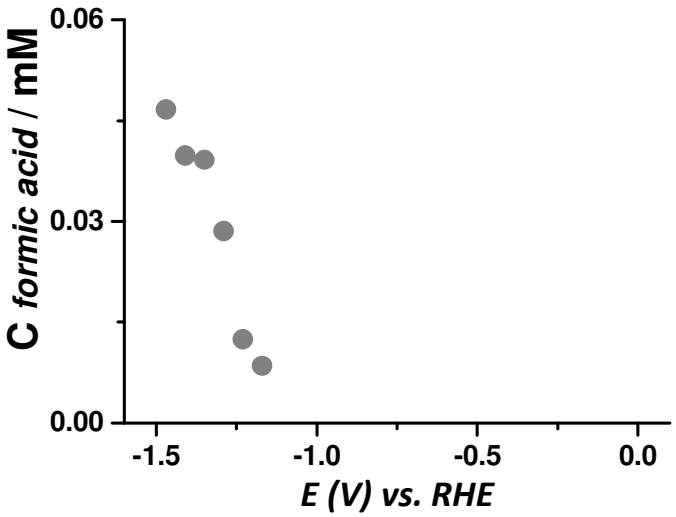

Figure AIII.7 Formation of formic acid on a polycrystalline palladium electrode detected with online HPLC using a phosphate buffer at pH 6.7 (0.1 M KH_2PO_4/ 0.1 M K_2HPO_4).

Appendix III.4 NMR spectroscopy

Table AIII.1 Liquid products identified with ^{1}H-NMR spectroscopy after 15 hours of CO_2 reduction at -1.2 V vs. RHE with a Pd-Au electrode in a 0.1 M KH_2PO_4 / 0.1 M K_2HPO_4 electrolyte (pH 6.7).

Assignment	Probed nucleus	Chemical shift (δ)	Multiplicity	J-coupling (Hz)	COSY cross peaks
Formate	$HCOO^-$	8.41	s		
Methanol	CH_3OH	3.31	s		
Ethanol	CH_3CH_2OH	3.61	q	6.4	1.13
Ethanol	CH_3CH_2OH	1.13	t	9.6	3.61
Acetate	CH_3COO^-	2.18	s		

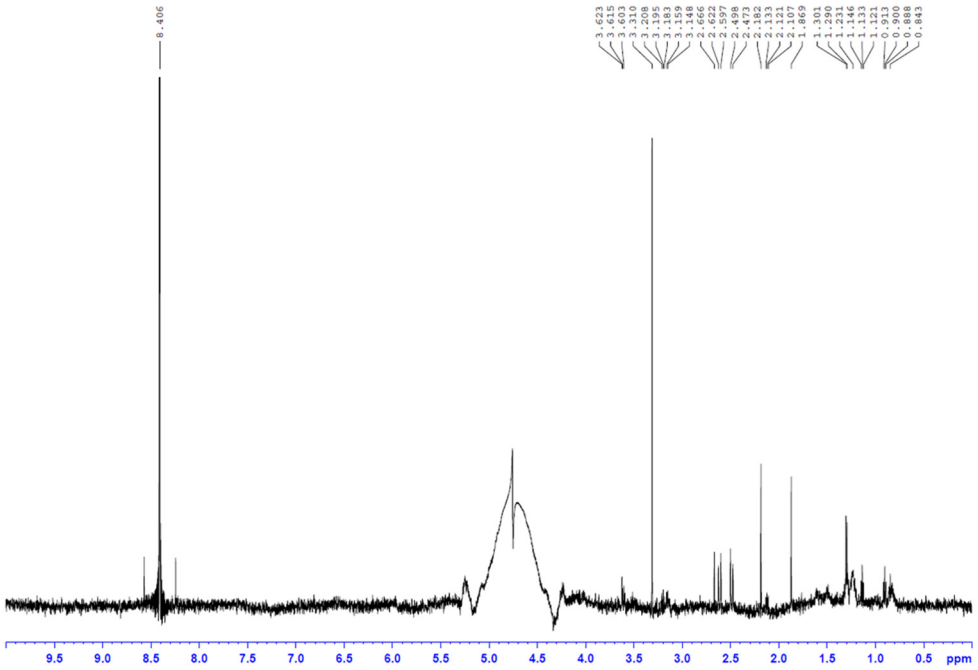

Figure AIII.8 Liquid products identified with ^{1}H-NMR spectroscopy after 15 hours of CO_2 reduction at -1.2 V vs. RHE with a Pd-Au electrode in a 0.1 M KH_2PO_4 / 0.1 M K_2HPO_4 electrolyte (pH 6.7).

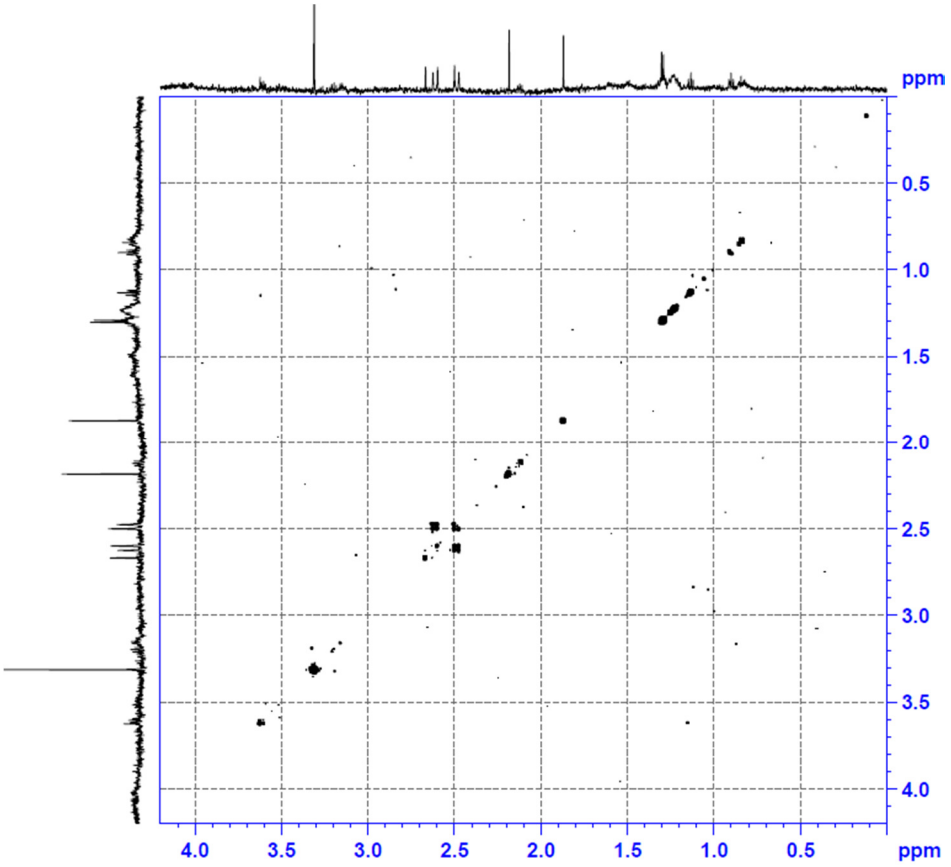

Figure AIII.9 COSY spectrum of a sample (sample to D_2O ratio = 9:1) of the catholyte compartment (0.1 M KH_2PO_4 / 0.1 M K_2HPO_4 electrolyte (pH 6.7)) after 15 hours of electrolysis with a Pd-Au electrode at -1.2 V vs. RHE.

Appendix III.5 IR compensation

Electrochemical impedance measurements were carried out prior to the long term electrolysis experiments to determine the resistance of the H-cell (see section S3). The impedance measurements were carried out using an Ivium A06075 potentiostat, at frequencies ranging from 10 kHz to 0.1 to measure the solution resistance. Since the resistance of the cell can vary for each experiment, it is important to correct for the resistance of the cell so that the applied potential during the electrolysis experiment corresponds to the intended electrode potential. A Nyquist plot was plotted as shown in Figure S10 and in the high-frequency part a linear fit was performed and the axis intersection was calculated. The value of this intersection represents the ohmic resistance of the cell. An average of 3 measurements was taken to calculate the value of R. Typically, very small resistances were measured, ranging from 4 to 12 Ω. This measured resistance was compensated for during the electrolysis experiments.

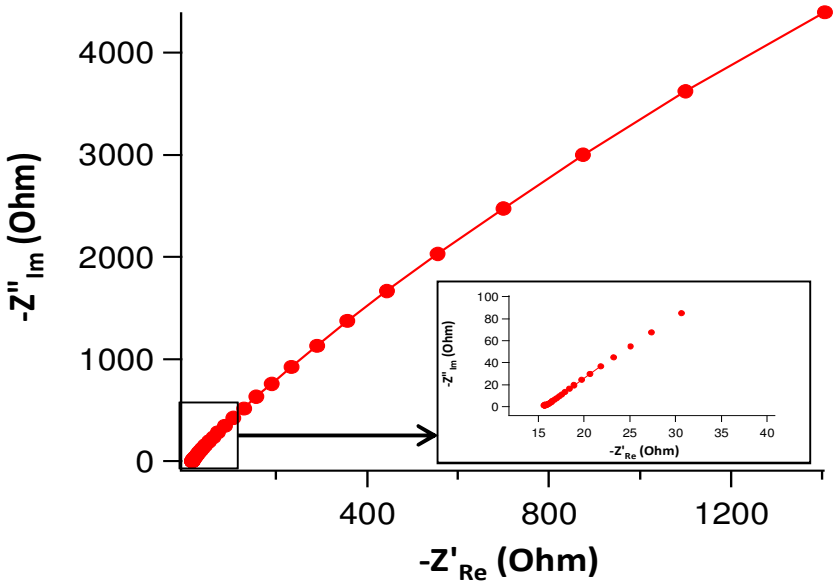

Figure AIII.10 Typical Nyquist plot used to calculate the resictance of the cell prior to electrolysis experiments.

Appendix III.6 Faradaic efficiencies on Pd-Au and 4MLs Pd on Au

Table AIII.2 Faradaic efficiencies toward C_1-C_3 hydrocarbons produced during CO_2 reduction on Pd-Au in a pH 6.7 phosphate buffer (0.1 M KH_2PO_4 / 0.1 M K_2HPO_4)

E (V) vs. RHE	CO (%)	CH_4 (%)	C_2H_4 (%)	C_2H_6 (%)	Σ C_2 (%)	C_3H_6 (%)	C_3H_8 (%)	Σ C_3 (%)
-0.4	19.62							
-0.5	24.07							
-0.6	30.92							
-0.7	18.26							
-0.8	9.62	0.92	0.08	0.23	0.31			
-0.9	9.00	1.26	0.10	0.28	0.38	0.09	0.03	0.12
-1.0	7.49	1.36	0.09	0.27	0.35	0.10	0.03	0.13
-1.1	6.77	1.54	0.10	0.35	0.45	0.10	0.03	0.14
-1.2	1.44	1.25	0.10	0.34	0.44	0.15	0.05	0.21
-1.3	1.75	1.49	0.14	0.40	0.53	0.19	0.06	0.25
-1.4	3.02	2.03	0.13	0.54	0.67	0.22	0.07	0.29
-1.5	6.70	1.16	0.13	0.42	0.55	0.21	0.07	0.28

Table AIII.3 Faradaic efficiencies toward C_4-C_5 hydrocarbons produced during CO_2 reduction on Pd-Au in a pH 6.7 phosphate buffer (0.1 M KH_2PO_4 / 0.1 M K_2HPO_4)

E (V) vs. RHE	Isobutane (%)	1-butene (%)	Butane (%)	Σ C_4 (%)	2-methyl-butane (%)	Pentene (%)	Pentane (%)	Σ C_5 (%)
-0.4								
-0.5								
-0.6								
-0.7								
-0.8								
-0.9								
-1	0.03	0.07	0.04	0.14				
-1.1	0.02	0.06	0.03	0.12				
-1.2	0.02	0.08	0.04	0.14	0.02	0.04	0.01	0.06
-1.3	0.03	0.09	0.04	0.16	0.01	0.02	0.00	0.04
-1.4	0.02	0.09	0.04	0.15	0.02	0.04	0.01	0.07
-1.5	0.02	0.08	0.04	0.14	0.01	0.04	0.01	0.06

Table AIII.4 Faradaic efficiencies toward C_1-C_3 hydrocarbons produced during CO_2 reduction on 4 Pd MLs on Au in a pH 6.7 phosphate buffer (0.1 M KH_2PO_4 / 0.1 M K_2HPO_4)

E (V) vs. RHE	CO (%)	CH_4 (%)	C_2H_4 (%)	C_2H_6 (%)	Σ C_2 (%)	C_3H_6 (%)	C_3H_8 (%)	Σ C_3 (%)
-0.4	80.86							
-0.5	81.43							
-0.6	73.77							
-0.7	60.63							
-0.8	27.23	4.48	0.38	1.16	1.54			
-0.9	14.17	2.82	0.33	1.00	1.33			
-1	5.34	2.90	0.21	0.74	0.95	0.11	0.28	0.39
-1.1	5.93	3.19	0.19	0.80	0.99	0.12	0.32	0.45
-1.2	8.47	3.30	0.18	0.77	0.95	0.12	0.32	0.44
-1.3	6.35	1.78	0.15	0.50	0.65	0.08	0.20	0.28
-1.4	4.33	1.07	0.10	0.31	0.41	0.05	0.12	0.17
-1.5	2.22	0.72	0.07	0.21	0.27	0.03	0.08	0.11

Table AIII.5 Faradaic efficiencies toward C_4-C_5 hydrocarbons produced during CO_2 reduction on 4 Pd MLs on Au in a pH 6.7 phosphate buffer (0.1 M KH_2PO_4 / 0.1 M K_2HPO_4)

E (V) vs. RHE	Isobutane (%)	1-butene (%)	Butane (%)	Σ C4 (%)	2-methyl-butane (%)	Pentene (%)	Pentane (%)	Σ C5 (%)
-0.4								
-0.5								
-0.6								
-0.7								
-0.8								
-0.9								
-1	0.02	0.05	0.12	0.19				
-1.1	0.02	0.06	0.14	0.22	0.02	0.02	0.06	0.11
-1.2	0.02	0.05	0.14	0.21	0.02	0.02	0.05	0.09
-1.3	0.01	0.02	0.06	0.10	0.02	0.02	0.04	0.07
-1.4	0.01	0.01	0.03	0.05	0.01	0.01	0.03	0.05
-1.5	0.01	0.01	0.03	0.05	0.01	0.01	0.02	0.03

Appendix III.7 Mono- and multilayer Pd deposition

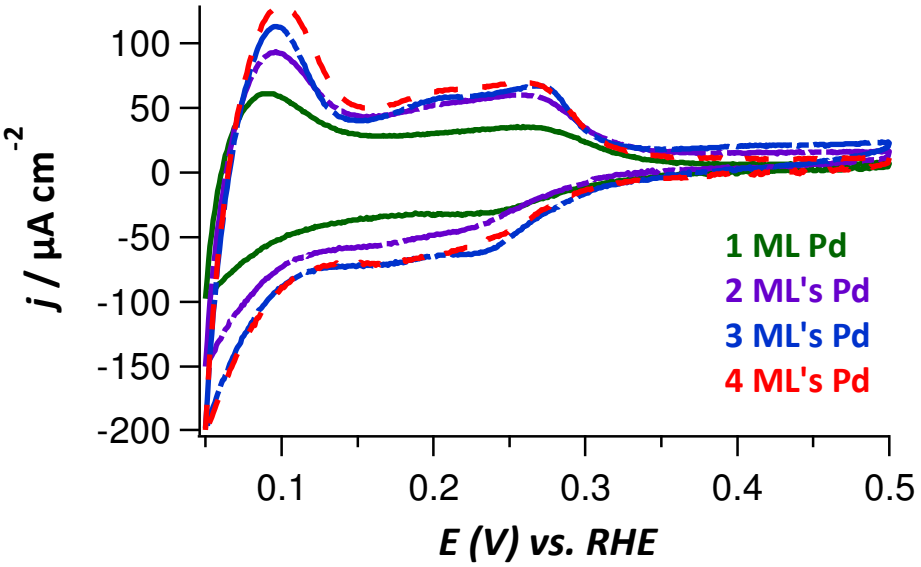

Figure AIII.11 Cyclic voltammograms of a polycrystalline gold electrode covered with 1 monolayer palladium (green line), 2 monolayers of palladium (purple dashed line), 3 monolayers of palladium (blue dashed line) and 4 monolayers of palladium (red dashed line) in a 0.5 M H_2SO_4 electrolyte purged with argon at a scan rate of 20 mV/s.

Appendix III.8 CO_2 reduction and blank voltammetry Pd MLs on Au

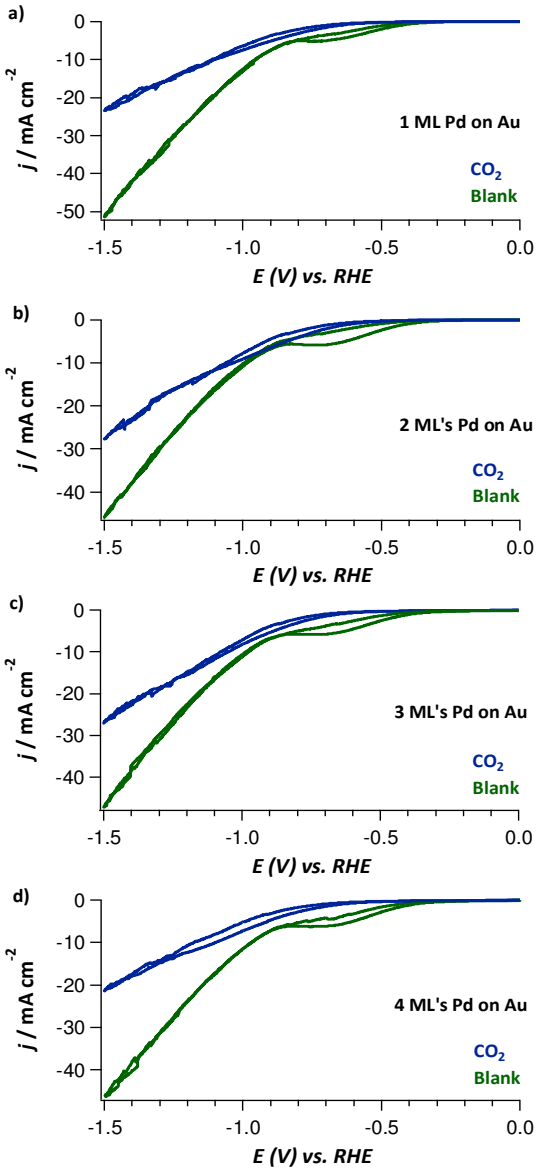

Figure AIII.12 Cyclic voltammograms of a polycrystalline gold electrode with diffent amounts of palladium monolayers recorded in a 0.1 M KH_2PO_4 / 0.1 M K_2HPO_4 electrolyte (pH 6.7) at a scan rate of 50 mV/s purged with either argon (green) or CO_2 (blue); **a)** 1 palladium monolayer; **b)** 2 palladium monolayers; **c)** 3 palladium monolayers; **d)** 4 palladium monolayers.

Appendix III.9 XPS data Au electrode

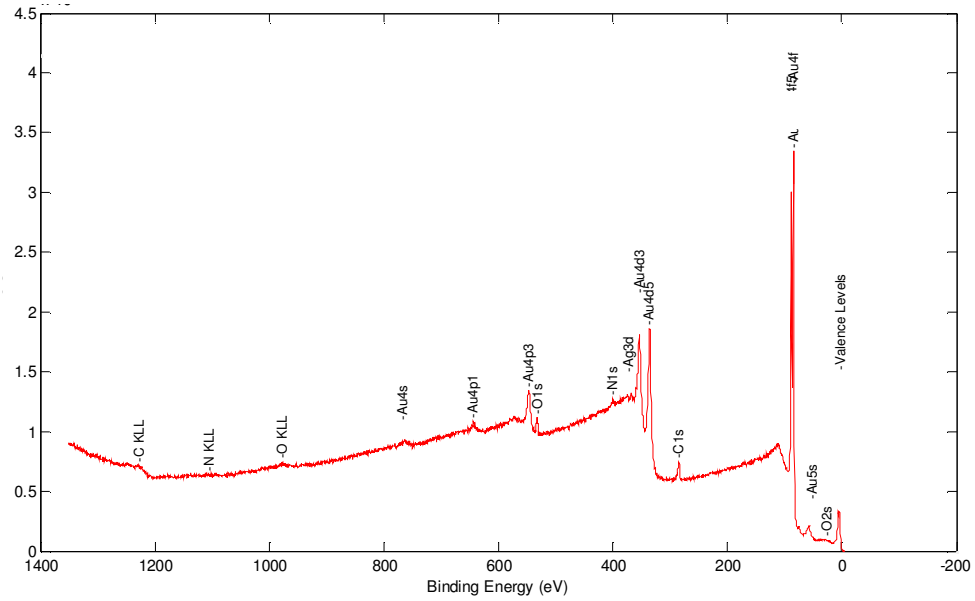

Figure AIII.13 XPS survey spectrum from -5 eV to 1345 eV of a gold electrode. Pass energy is 224 eV and δE is 0.4 eV.

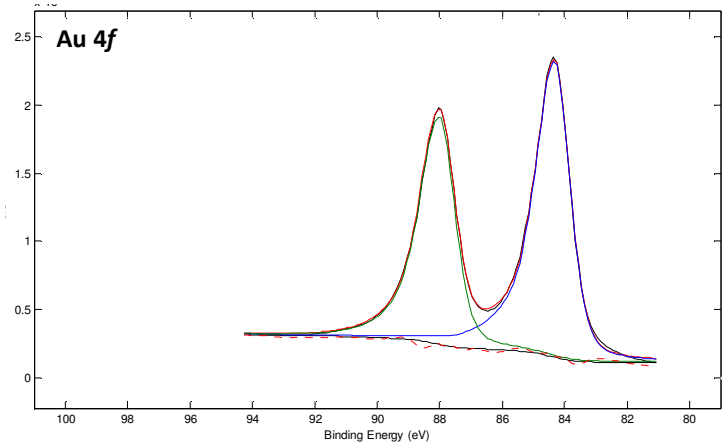

Figure AIII.14 Au 4*f* spectral region in XPS for a gold electrode.

Appendix III.10 XPS data PdAu electrode

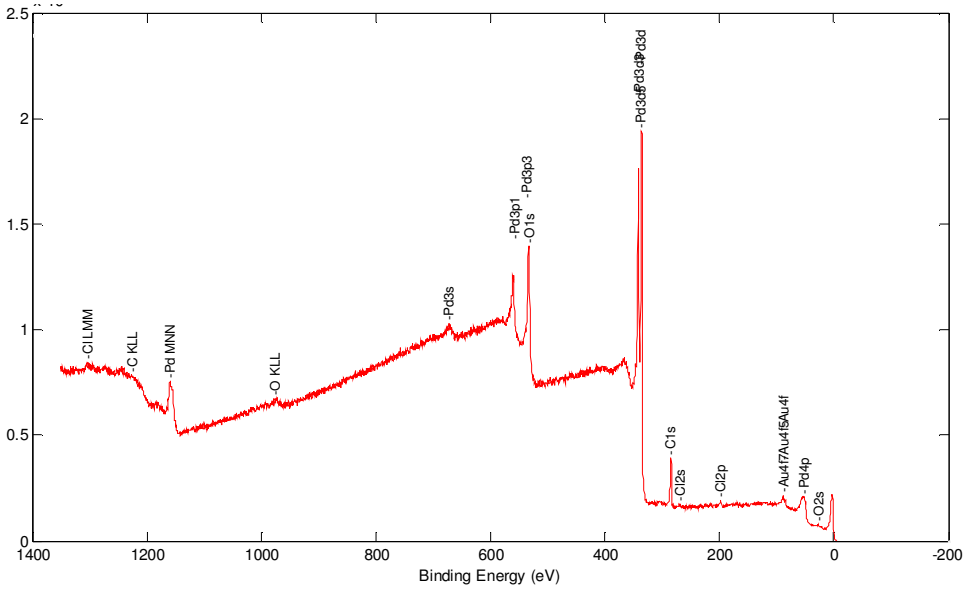

Figure AIII.15 XPS survey spectrum from -5 eV to 1345 eV of a Pd-Au electrode. Pass energy is 224 eV and δE is 0.4 eV.

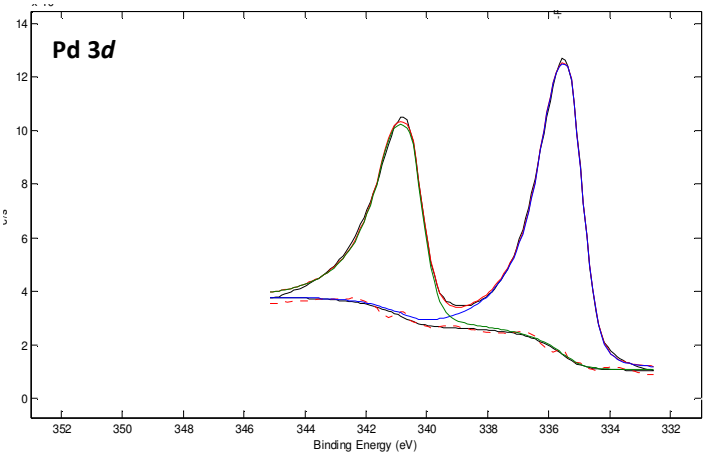

Figure AIII.16 Pd 3*d* spectral region in XPS for a Pd-Au electrode.

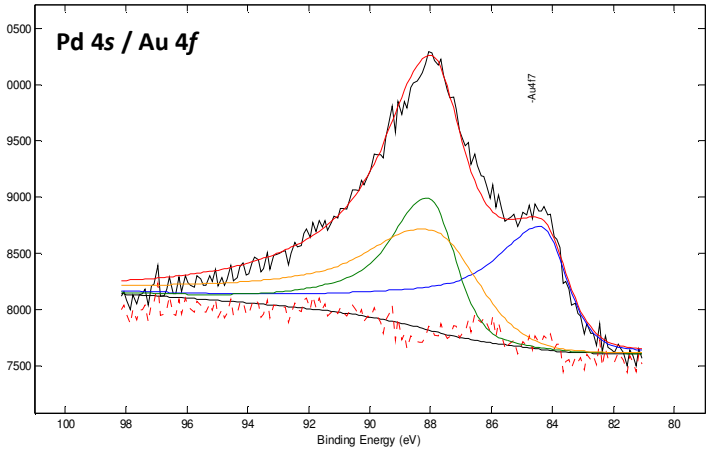

Figure AIII.17 Pd 4*s* and Au 4*f* spectral region in XPS for a Pd-Au electrode.

Appendix III.11 XPS data PdAu electrode after electrolysis

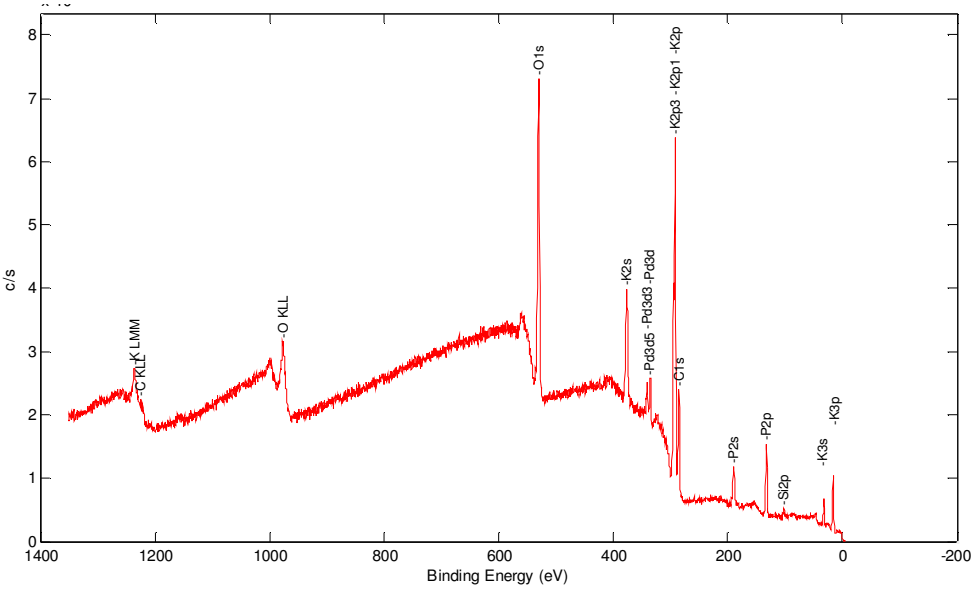

Figure AIII.18 XPS survey spectrum from -5 eV to 1345 eV of a Pd-Au electrode after 30 minutes of electrolysis at -1.2 V vs. RHE. Pass energy is 224 eV and δE is 0.4 eV.

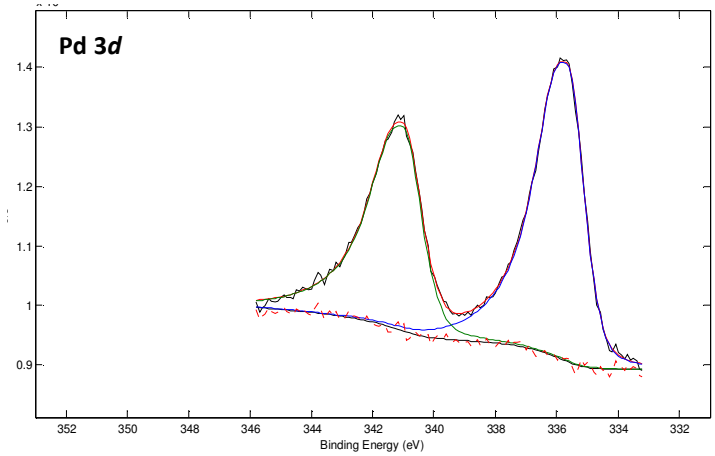

Figure AIII.19 Pd 3*d* spectral region in XPS for a Pd-Au electrode after 30 minutes of electrolysis at -1.2 V vs. RHE.

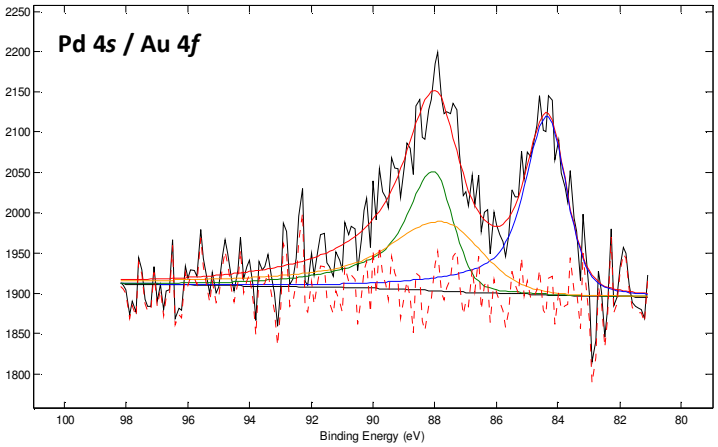

Figure AIII.20 Pd 4*s* and Au 4*f* spectral region in XPS for a Pd-Au electrode after 30 minutes of electrolysis at -1.2 V vs. RHE.

Appendix III.12 XPS data for an Au electrode with 4 MLs Pd

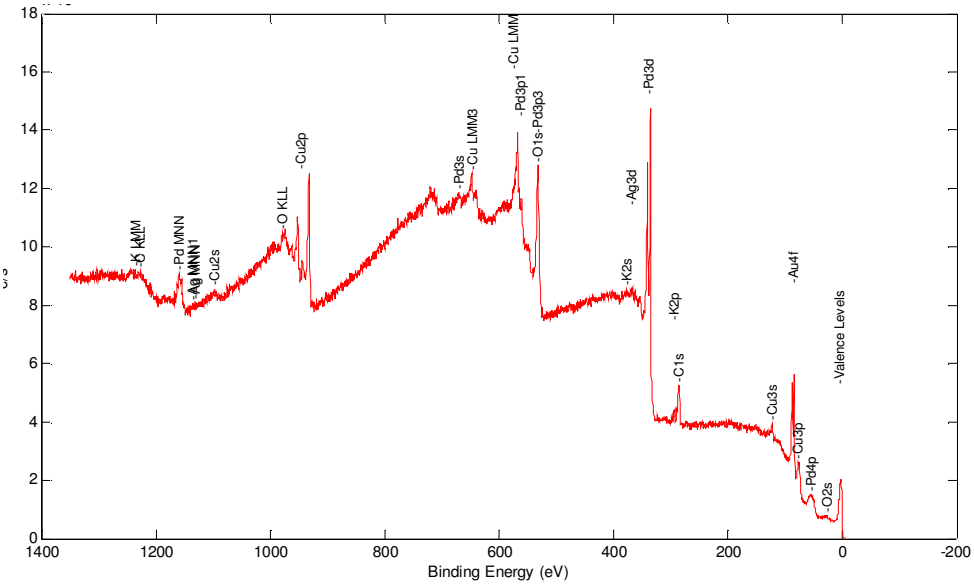

Figure AIII.21 XPS survey spectrum from -5 eV to 1345 eV of an Au electrode covered with 4 Pd MLs. Pass energy is 224 eV and δE is 0.4 eV.

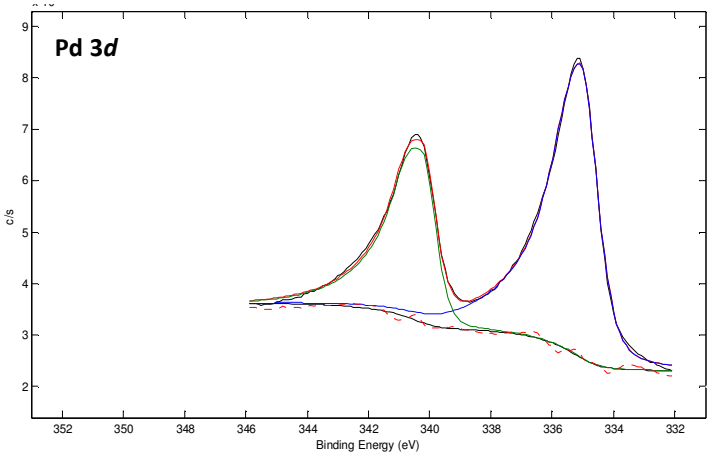

Figure AIII.22 Pd 3*d* spectral region in XPS of an Au electrode covered with 4 Pd MLs.

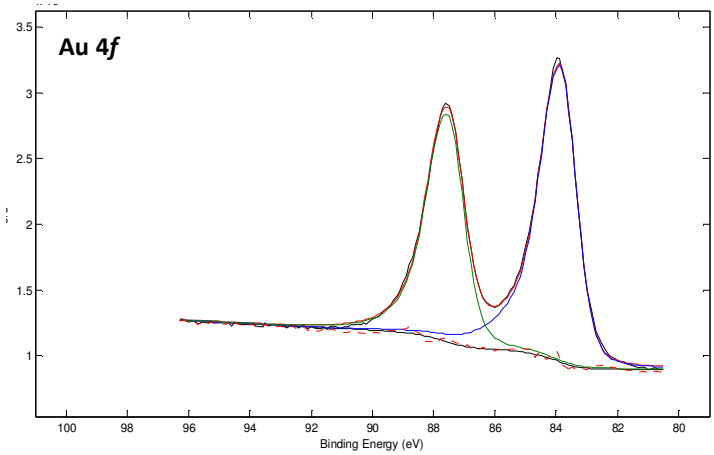

Figure AIII.23 Au 4*f* spectral region in XPS of an Au electrode covered with 4 Pd MLs.

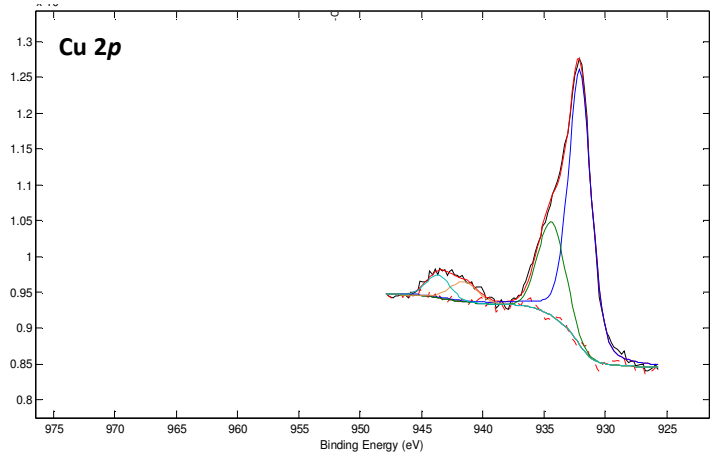

Figure AIII.24 Cu 2*p* spectral region in XPS of an Au electrode covered with 4 Pd MLs.

Appendix III.13 XPS data for an Au electrode with 4 MLs Pd after electrolysis

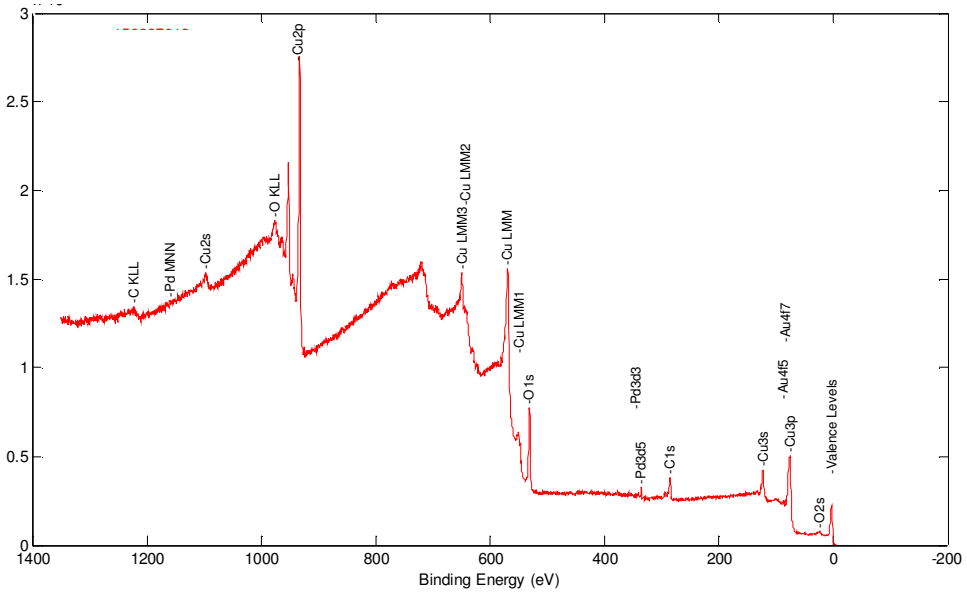

Figure AIII.25 XPS survey spectrum from -5 eV to 1345 eV of an Au electrode covered with 4 Pd MLs after 30 minutes of electrolysis at -1.2 V vs. RHE. Pass energy is 224 eV and δE is 0.4 eV.

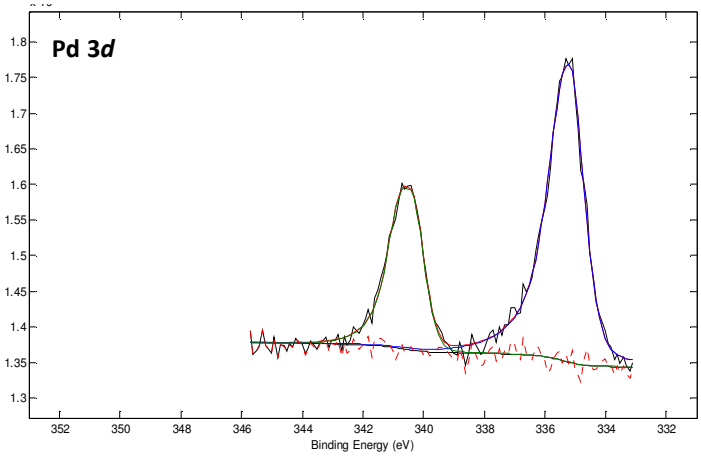

Figure AIII.26 Pd 3*d* spectral region in XPS of an Au electrode covered with 4 Pd MLs after 30 minutes of electrolysis at -1.2 V vs. RHE.

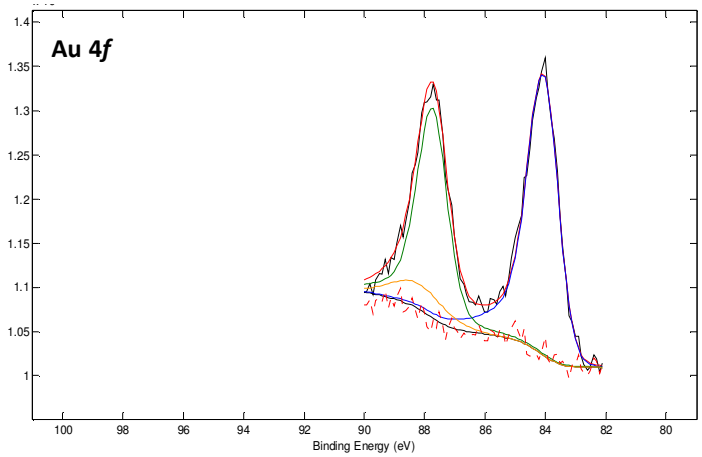

Figure AIII.27 Au 4*f* spectral region in XPS of an Au electrode covered with 4 Pd MLs after 30 minutes of electrolysis at -1.2 V vs. RHE.

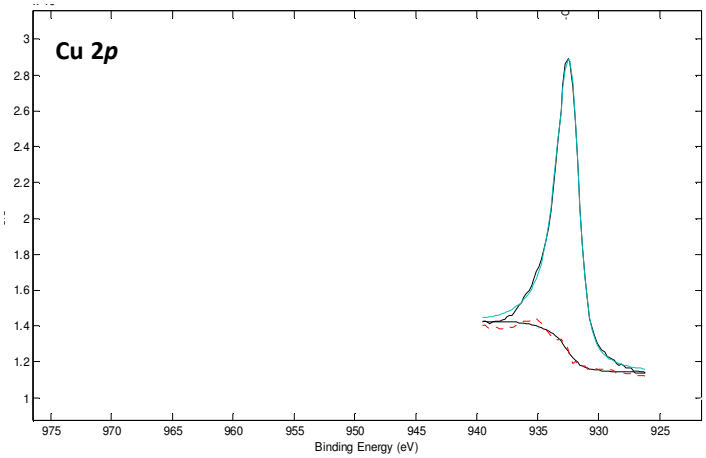

Figure AIII.28 Cu 2*p* spectral region in XPS of an Au electrode covered with 4 Pd MLs after 30 minutes of electrolysis at -1.2 V vs. RHE.

Appendix IV

Supporting information to Chapter 7

Appendix IV.1 X-ray diffraction

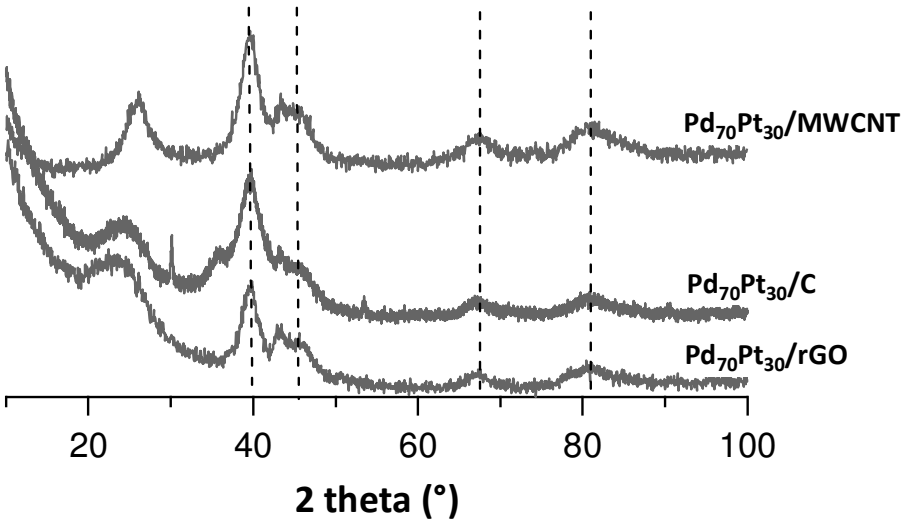

Figure AIV.1 X-ray diffraction spectra of $Pd_{70}Pt_{30}$ nanoparticles on different support materials; multi-walled carbon nanotubes (MWCNT), Vulcan XC-72 (C) and reduced graphene oxide (rGO).

Appendix IV.2 IR compensation

Electrochemical impedance measurements were carried out prior to the long term electrolysis experiments to determine the resistance of the H-cell (see section S3). The impedance measurements were carried out using an Ivium A06075 potentiostat, at frequencies ranging from 10 kHz to 0.1 to measure the solution resistance. Since the resistance of the cell can vary for each experiment, it is important to correct for the resistance of the cell so that the applied potential during the electrolysis experiment corresponds to the intended electrode potential. A Nyquist plot was plotted as shown in Figure S3 and in the high-frequency part a linear fit was performed and the axis intersection was calculated. The value of this intersection represents the ohmic resistance of the cell. An average of 3 measurements was taken to calculate the value of R. Typically, very small resistances were measured, ranging from 3 to 10 Ω. This resistance was compensated for during the electrolysis experiments.

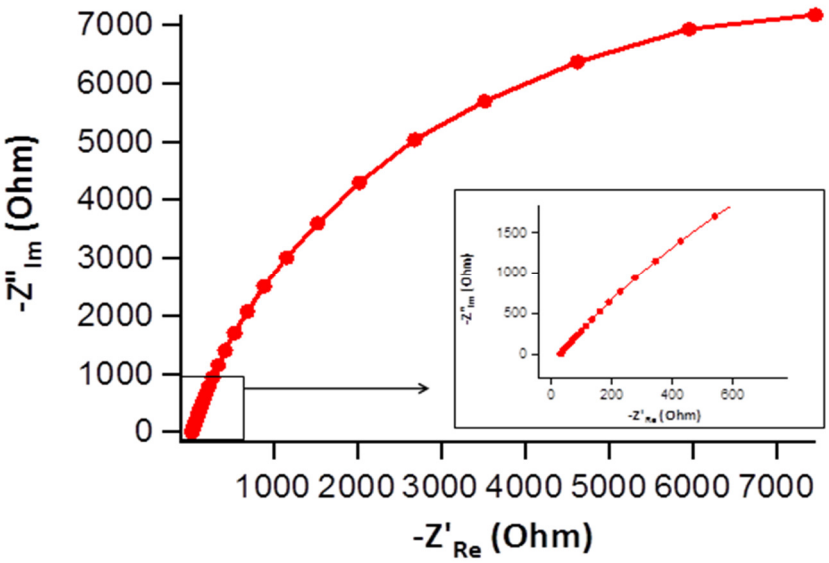

Figure AIV.2 Typical Nyquist plot used to calculate the resictance of the cell prior to electrolysis experiments.

Appendix IV.3 Faradaic efficiency

Faradaic efficiency measurements were performed in a custom-made H-cell over the course of 2 hours. Every 10 minutes a sample of 100 µl was taken from the cathodic compartment. These samples were analyzed with HPLC to determine the concentration of formic acid. During the 10 minutes of electrolysis current-time plots were made, that were used afterwards to calculate the total charge (C) that was consumed. Since every molecule of formic acid is produced from CO_2 requires 2 e^-, the charge corresponding to formic acid production can be calculated from the amount of formic acid that was produced in the entire volume of the cell multiplied by 2 times the elementary charge (e). The faradaic efficiency was then determined by dividing this charge for formic acid formation by the total amount of charge that was consumed, as shown in Equation 1. The FE was calculated for the different nanoparticle compositions.

$$FE = \frac{[\text{Formic Acid}] \cdot 2e}{\sum \text{Charge}} \cdot 100\% \quad (1)$$

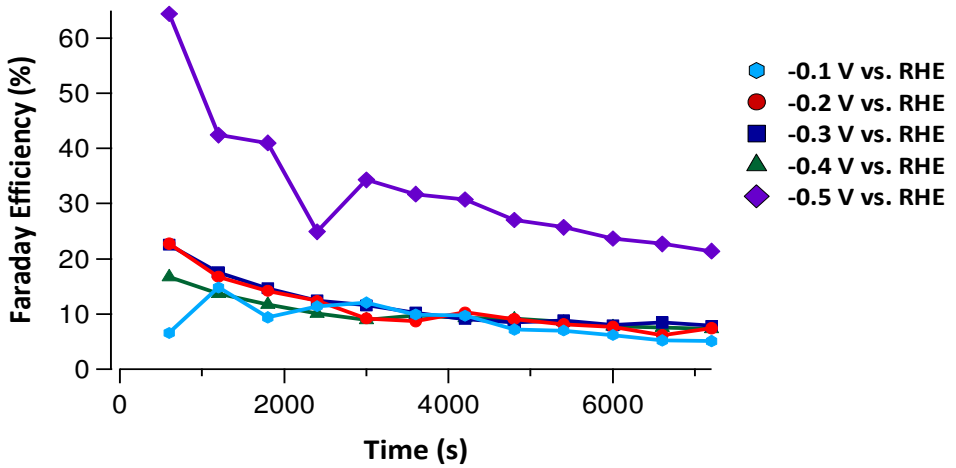

Figure AIV.3 Faradaic efficiencies for formic acid production from CO_2 on $Pd_{70}Pt_{30}$ nanoparticles on a reduced graphene oxide (rGO) support in a 0.1 M K_2HPO_4 / 0.1 KH_2PO_4 electrolyte (pH 6.7) that was saturated with CO_2 at potentials ranging from 0 V vs. RHE to -0.5 V vs. RHE (the applied potential was corrected for the cell resistance). The experiments were conducted for 2 hours, while samples of the electrolyte were taken every 10 minutes.

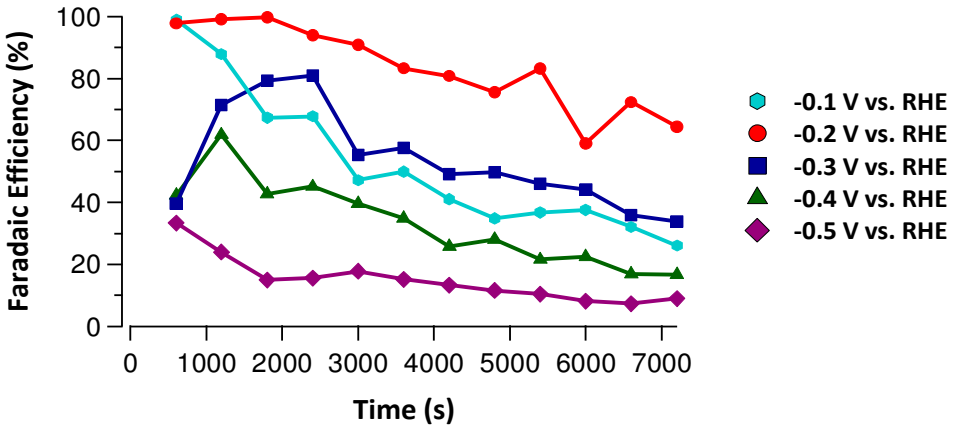

Figure AIV.4 Faradaic efficiencies for formic acid production from CO_2 on $Pd_{70}Pt_{30}$ nanoparticles on a multi-walled carbon nanotube (MWCNT) support in a 0.1 M K_2HPO_4 / 0.1 KH_2PO_4 electrolyte (pH 6.7) that was saturated with CO_2 at potentials ranging from 0 V vs. RHE to -0.5 V vs. RHE (the applied potential was corrected for the cell resistance). The experiments were conducted for 2 hours, while samples of the electrolyte were taken every 10 minutes.

Table AIV.1 Tabulated faradaic efficiency values for CO_2 reduction to formic acid on $Pd_{70}Pt_{30}$ nanoparticles on reduced graphene oxide (rGO) as support at different potentials over the course of 2 hours.

Time (s)	**-0.1 V vs. RHE** FE (%)	**-0.2 V vs. RHE** FE (%)	**-0.3 V vs. RHE** FE (%)	**-0.4 V vs. RHE** FE (%)	**-0.5 V vs. RHE** FE (%)
600	6.6	22.7	22.5	16.7	64.4
1200	14.8	16.8	17.6	13.6	42.4
1800	9.4	14.2	14.6	11.8	41.0
2400	11.4	12.4	12.4	10.1	24.9
3000	12.1	9.2	11.6	9.0	34.3
3600	9.9	8.7	10.2	9.7	31.7
4200	9.7	10.3	9.1	9.3	30.7
4800	7.2	9.1	8.4	9.1	27.0
5400	7.0	8.1	8.8	8.5	25.7
6000	6.2	7.7	8.0	7.8	23.7
6600	5.2	6.2	8.5	7.6	22.7
7200	5.1	7.4	7.9	7.3	21.4

Table AIV.2 Tabulated faradaic efficiency values for CO_2 reduction to formic acid on $Pd_{70}Pt_{30}$ nanoparticles on multi-walled carbon nanotubes (MWCNT) as support at different potentials over the course of 2 hours.

Time (s)	**-0.1 V vs. RHE** FE (%)	**-0.2 V vs. RHE** FE (%)	**-0.3 V vs. RHE** FE (%)	**-0.4 V vs. RHE** FE (%)	**-0.5 V vs. RHE** FE (%)
600	98.9	97.8	39.7	42.4	33.4
1200	87.9	99.1	71.4	61.9	24.0
1800	67.4	99.8	79.3	42.8	15.0
2400	67.8	94.0	80.9	45.1	15.6
3000	47.2	90.8	55.4	39.6	17.8
3600	49.9	83.3	57.5	35.0	15.2
4200	41.1	80.8	49.2	25.9	13.3
4800	34.9	75.5	49.8	28.1	11.6
5400	36.8	83.2	46.0	21.6	10.5
6000	37.6	59.1	44.2	22.5	8.1
6600	32.1	72.4	35.9	16.9	7.3
7200	26.1	64.4	33.9	16.7	9.0

Appendix IV.4 TEM data of $Pd_{70}Pt_{30}$ nanoparticles

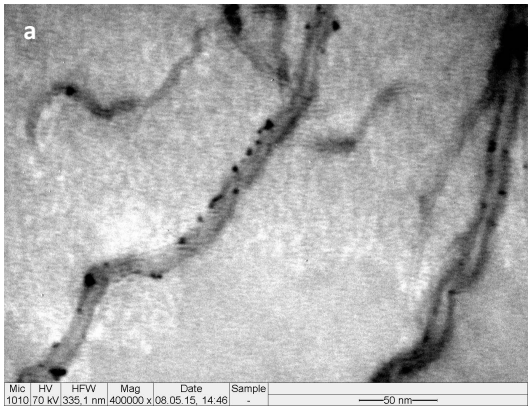

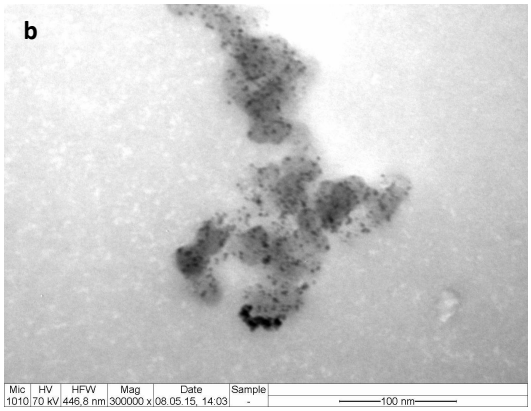

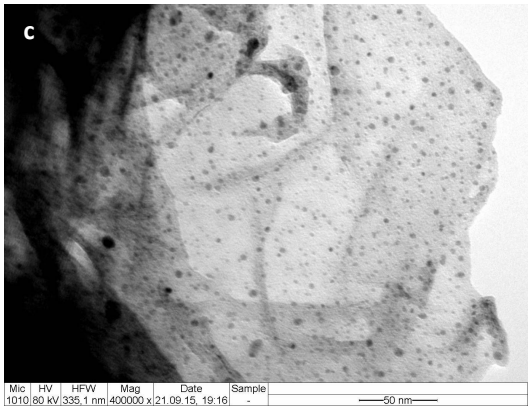

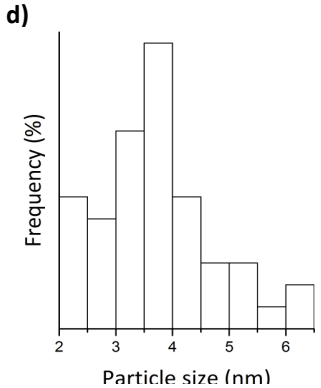

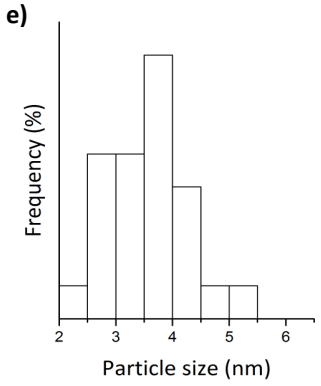

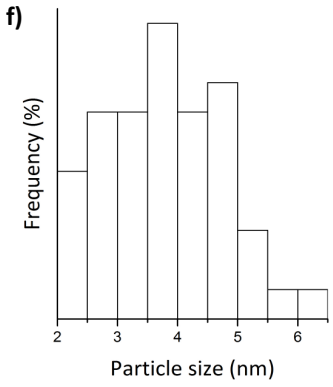

Figure AIV.5 Transmission electron microscopy (TEM) images of: **a)** $Pd_{70}Pt_{30}$/MWCNT, **b)** $Pd_{70}Pt_{30}$/C, **c)** $Pd_{70}Pt_{30}$/rGO, and particle size distributions for; **d)** $Pd_{70}Pt_{30}$/MWCNT, **e)** $Pd_{70}Pt_{30}$/C and **f)** $Pd_{70}Pt_{30}$/rGO.

Appendix IV.5 CO_2 reduction and blank voltammetry on $Pd_{70}Pt_{30}$

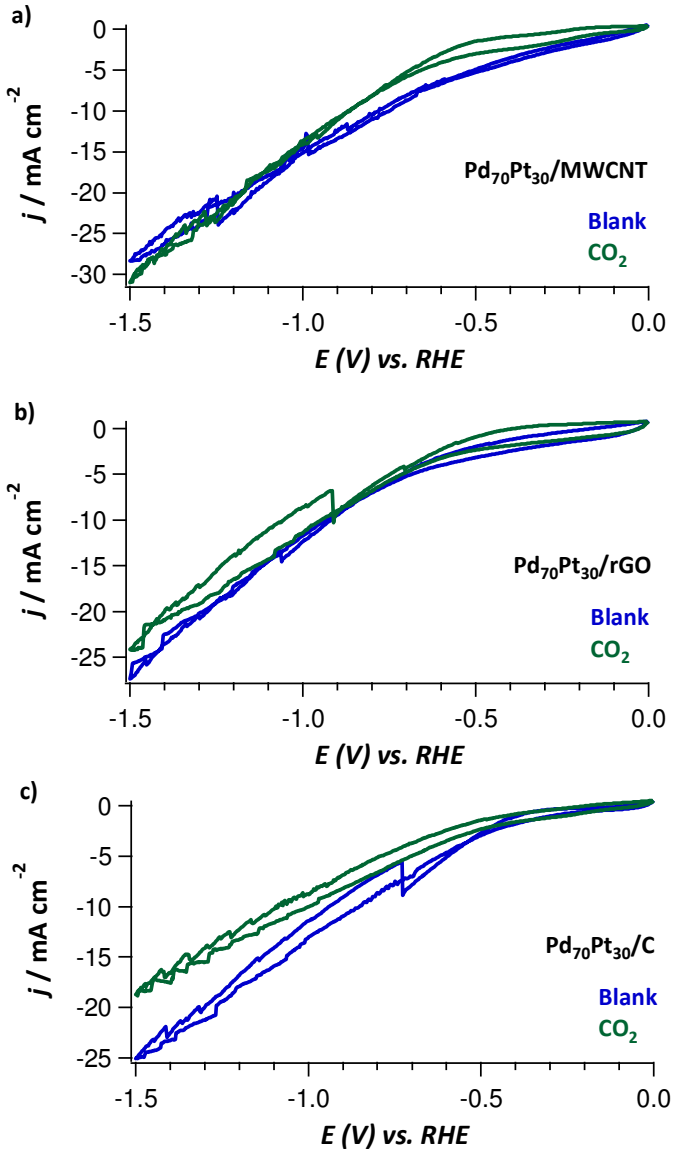

Figure AIV.6 Cyclic voltammograms of **a)** $Pd_{70}Pt_{30}$/MWCNT nanoparticles, **b)** $Pd_{70}Pt_{30}$/MWCNT nanoparticles and **c)** $Pd_{70}Pt_{30}$/C nanoparticles recorded in a 0.1 M KH_2PO_4 / 0.1 M K_2HPO_4 electrolyte (pH 6.7) at a scan rate of 50 mV/s purged with either argon (blue lines) or CO_2 (green lines).